Bioorganic Chemistry 88 (2019) 102954

Contents lists available at ScienceDirect

Bioorganic Chemistry

journal homepage: www.elsevier.com/locate/bioorg

Synthesis, characterization, anticancer evaluation and mechanisms of cytotoxic activity of novel 3-hydroxy-3-pyrrolin-2-ones bearing thenoyl fragment: DNA, BSA interactions and molecular docking study

Nenad Joksimović[a], Jelena Petronijević[a], Nenad Janković[a], Dejan Baskić[b], Suzana Popović[b], Danijela Todorović[c], Sanja Matić[d], Goran A. Bogdanović[e], Milan Vraneš[f], Aleksandar Tot[f], Zorica Bugarčić[a,*]

[a] University of Kragujevac, Faculty of Science, Department of Chemistry, Radoja Domanovića 12, 34000 Kragujevac, Serbia
[b] University of Kragujevac, Faculty of Medical Sciences, Centre for Molecular Medicine and Stem Cell Research, Svetozara Markovića 69, 34000 Kragujevac, Serbia
[c] University of Kragujevac, Faculty of Medical Sciences, Department of Genetics, Svetozara Markovića 69, 34000 Kragujevac, Serbia
[d] Doctoral Academic Study, Faculty of Medical Sciences, University of Kragujevac, Svetozara Markovica 69, 34000 Kragujevac, Serbia
[e] Vinča Institute of Nuclear Science University of Belgrade, P.O. Box 522, 11001 Belgrade, Serbia
[f] University of Novi Sad, Department of Chemistry, Biochemistry and Environmental Protection, Trg Dositeja Obradovića 3, 21000 Novi Sad, Serbia

ARTICLE INFO

Keywords:
3-Hydroxy-3-pyrrolin-2-ones
Mechanisms of cytotoxic activity
Antitumor activity
DNA binding study
BSA binding study
Molecular docking

ABSTRACT

In order to make a progress in discovering a new agents for chemotherapy with improved properties and bearing in mind the fact that substituted 3-hydroxy-3-pyrrolin-2-ones belong to a class of biologically active compounds, series of novel 1,5-diaryl-4-(2-thienylcarbonyl)-3-hydroxy-3-pyrrolin-2-ones were synthesized and characterized by spectral (UV–Vis, IR, NMR, ESI-MS), X-ray and elemental analysis. All compounds were examined for their cytotoxic effect on human cancer cell lines HeLa and MDA-MB 231 and normal fibroblasts (MRC-5). Four compounds, 3-hydroxy-1-(p-tolyl)-4-(2-thienylcarbonyl)-5-(4-chlorophenyl)-2,5-dihydro-1H-pyrrol-2-one (**D10**), 3-hydroxy-1-(3-nitrophenyl)-4-(2-thienylcarbonyl)-5-(4-(benzyloxy)phenyl)-2,5-dihydro-1H-pyrrol-2-one (**D13**), 3-hydroxy-1-(4-nitrophenyl)-4-(2-thienylcarbonyl)-5-(4-(benzyloxy)phenyl)-2,5-dihydro-1H-pyrrol-2-one (**D14**), and 3-hydroxy-1-(4-chlorophenyl)-4-(2-thienylcarbonyl)-5-(4-(benzyloxy)phenyl)-2,5-dihydro-1H-pyrrol-2-one (**D15**), that showed the highest cytotoxicity against malignant cells and the best selectivity towards normal cells were selected for further experiments. Results obtained by investigating mechanisms of cytotoxic activity suggest that selected 3-hydroxy-3-pyrrolin-2-one derivatives in HeLa cells induce apoptosis that is associated with S phase arrest (**D13**, **D15**, and **D10**) or unrelated to cell cycle distribution (**D14**). Additionally, to better understand their suitability for potential use as anticancer medicaments we studied the interactions between biomacromolecules (DNA or BSA) and **D13** and **D15**. The results indicated that **D13** and **D15** have great affinity to displace EB from the EB-DNA complex through intercalation [K_{sv} = (3.7 ± 0.1) and (3.4 ± 0.1) × 10^3 M^{-1}, respectively], an intercalative mode also confirmed through viscosity measurements. K_a values, obtained as result of fluorescence titration of BSA with **D13** and **D15** [K_a = (4.2 ± 0.2) and (2.6 ± 0.2) × 10^5 M, respectively], support the fact that a significant amount of the tested compounds could be transported and distributed through the cells. In addition, by DNA and BSA molecular docking study for **D13, D14** and **D15** is determined and predicted the binding mode and the interaction region.

1. Introduction

One of the biggest health problem in our society and one of the primary targets in medicinal chemistry nowadays is cancer. Since the discovery of cisplatin and its use in clinical therapy, scientists have made a lot of effort to synthesize many platinum-based drugs that could be less toxic to healthy tissue [1–3] and to overcome the resistance of some tumors to cisplatin [4,5]. The main goal for developing non-platinum anticancer drugs is to overcome the limits of platinum drugs: severe toxicity on healthy tissue, narrow range of activity and after treatment acquired resistance [1–5]. The discovery of new nonplatinum drugs with less side effects is of the major interest in pharmaceutical

* Corresponding author.
E-mail address: zoricab@kg.ac.rs (Z. Bugarčić).

https://doi.org/10.1016/j.bioorg.2019.102954
Received 28 January 2019; Received in revised form 3 April 2019; Accepted 25 April 2019
Available online 27 April 2019

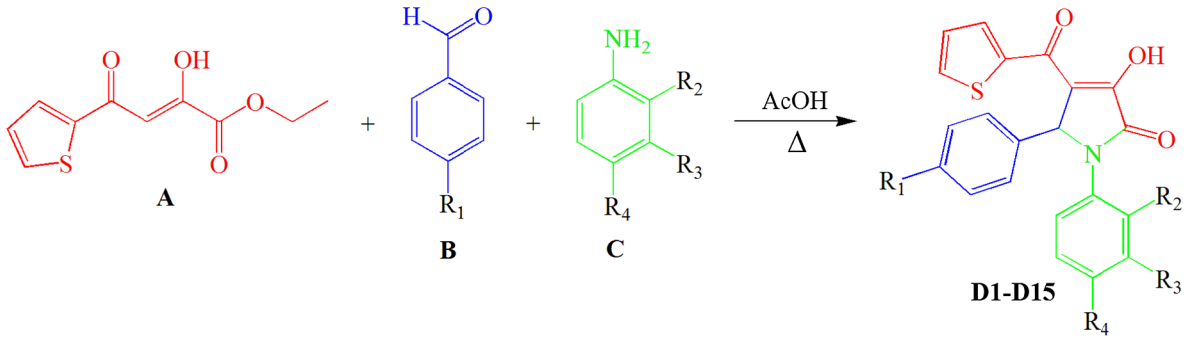

D1 R_1=R_3=R_4= H, R_2= CH_3
D2 R_1=R_2=R_3= H, R_4= CH_3
D3 R_1=R_2=R_3= H, R_4= OH
D4 R_1=R_2=R_3= H, R_4= Cl
D5 R_1=R_2=R_3= H, R_4= Br
D6 R_1=R_2=R_3= H, R_4= I
D7 R_1= NO_2, R_2=R_3= H, R_4= Cl
D8 R_1= NO_2, R_2=R_3= H, R_4= Br
D9 R_1= NO_2, R_2=R_3= H, R_4= I
D10 R_1= Cl, R_2=R_3= H, R_4= CH_3
D11 R_1= Cl, R_2=R_3= H, R_4= Cl
D12 R_1= Cl, R_2=R_3= H, R_4= Br
D13 R_1= OCH_2Ph, R_2=R_4= H, R_3= NO_2
D14 R_1= OCH_2Ph, R_2=R_3= H, R_4= NO_2
D15 R_1= OCH_2Ph, R_2=R_3= H, R_4= Cl

Scheme 1. General synthetic pathway towards 1,5-diaryl-4-(2-thienylcarbonyl)-3-hydroxy-3-pyrrolin-2-ones (**D1-D15**).

chemistry [6]. Substituted 3-hydroxy-3-pyrrolin-2-ones belong to a class of biologically active compounds. They can be obtained in the reaction between ethyl-2-hydroxy-4-thienyl-4-oxo-2-butenoate with a mixture of aryl(alkyl)amine and an aldehyde by short-term heating of a mixture of starting reagents [7]. These compounds possess different types of pharmacological activities [8]. For example, some investigations showed that they have good antimicrobial activity [9–12]. Also, these compounds have many other biological activities such as anti-inflammatory, antiviral, antifungal, and nootropic [13–15]. To sum up, various biologically active natural products containing either 3-acyl-5-hydroxy-3-pyrrolin-2-one or 3-acyl-3,4-epoxy-5-hydroxypyrrolidin-2-one are isolated, suggesting that the pyrrolidinone moiety is mostly responsible for the biological activity of these compounds.

In order to discover new anticancer agents with improved properties and bearing in mind previous facts, we studied three-component, the one-pot reaction of acylpyruvic acid ethyl ester with a mixture of an aromatic aldehyde and aromatic amine to produce novel potential antitumor drugs. It was found that reaction between above-mentioned substrates, in glacial acetic acid as solvent, lead to the formation of 1,5-diaryl-4-(2-thienylcarbonyl)-3-hydroxy-3-pyrrolin-2-ones (Scheme 1). The fifteen 1,5-diaryl-4-(2-thienylcarbonyl)-3-hydroxy-3-pyrrolin-2-ones were exposed to cytotoxic evaluation, fluorescence measurements and molecular docking studies. In addition, the potential mechanism of cytotoxic activity of some 3-hydroxy-3-pyrrolin-2-one derivates was investigated.

Fluorescence spectroscopy is an excellent experimental method to study interactions between biomacromolecules (DNA, carrier proteins, *etc.*) and small drugs such as presented compounds. The investigations on the interaction of small drugs with deoxyribonucleic acid are of great interest due to their potential use as anticancer medicaments [16–18]. In general, small molecules can interact with DNA through covalent interactions (interstrand/intrastrand cross-linking) [19–21] or via noncovalent associations (stacking [22–24], groove binding [25,26], intercalation [27]). Bovine serum albumin (BSA) is the protein that has the ability to transport a large number of endogenous and exogenous ligands such as amino acids, fatty acids, steroids, metal ions, and drugs in the bloodstream. Therefore, it is important to investigate drug-protein interactions due to structural similarities of BSA with human serum albumin (HSA) [28].

2. Results and discussion

2.1. Synthesis and characterization

We used the three-component reaction between acylpyruvic acid ethyl ester, (*Z*)-ethyl 2-hydroxy-4-oxo-4-(thiophen-2-yl)but-2-enoate (**A**), and a mixture of differently substituted aromatic aldehyde (**B**) and an aromatic amine (**C**) to synthesize fifteen 1,5-diaryl-4-(2-thienylcarbonyl)-3-hydroxy-3-pyrrolin-2-ones (**D1-D15**), fourteen novel and one previously reported. All the compounds are obtained in glacial acetic acid as catalyst and solvent, by the procedure described earlier [29] with minor corrections of reaction conditions.

All synthesized novel compounds were characterized by UV–Vis, NMR (^{1}H and ^{13}C spectra of compounds **D1-D15** are presented in the ESI, Figs. S1–S30), MS spectroscopy and elemental analysis. For one, compound **D2** that crystallized from DMSO solution, crystal structure was determined by using single-crystal X-ray diffraction analysis.

2.1.1. Crystal and molecular structures of *D2*

Single-crystal X-ray diffraction analysis has shown that the **D2** compound crystallized with two molecules of DMSO (Fig. 1). The existence of two carbonyl groups (the C1—O1 and C5—O3) and one hydroxyl (the C2—O2H) is clearly confirmed. The central N1 five-membered ring is almost ideally planar (root-mean-square deviation of fitted atoms is 0.012 Å). This ring forms a dihedral angle of 16.9(1)° with neighboring C16—C21 phenyl ring. The C5—O3 carbonyl group is directed between the N1 and S1 five-membered rings [the C4—C3—C5—O3 and O3—C5—C6—S1 torsion angles are −16.1(3) and −18.0(3)° respectively] approximately bisecting the dihedral angle between these two heterocycles. With a dihedral angle of 89.2(1)° the C10—C15 phenyl ring is almost perfectly placed in an orthogonal position relating to the central N1 ring.

The C2—C3 bond with the bond length of 1.341(3) Å (Table S1) is the shortest C—C bond in the whole molecule while the longest one is C4—C10 [1.522(3) Å]. The N1 is clearly an sp^2 hybridized atom since that the sum of bond angles around this atom is 359.9° and all N—C bonds are coplanar. The N1 forms three N—C bonds with significantly different bond lengths (Table S1). The shortest N1—C1 bond with an interatomic distance of 1.369(3) Å probably enables electron π delocalization across the N1—C1—O1 fragment.

The O2—H…O4^i is only one classical intermolecular hydrogen bond in the crystal structure of **D2**, however, it has quite short H…O distance of 1.78(3) Å [O2—H = 0.80(3) Å, O2…O3^i = 2.538(3) Å, O2—H…O3^i = 159(3)°; symmetry code: (i) x + 1, y, z]. The C1—O1 and C5—O3 carbonyl groups form only very weak C—H…O hydrogen bonds with H…O distance longer than 2.55 Å. Intermolecular C—H…π interactions dominate in the crystal packing by their frequency. Thus in Fig. 1 one can see that the methyl groups from two DMSO molecules are directed to the centers of neighboring π systems.

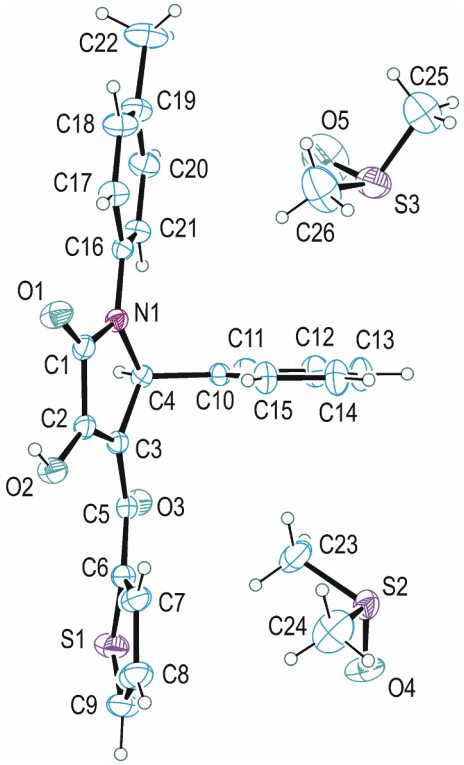

Fig. 1. Crystal structure and atom-numbering scheme of **D2**. Displacement ellipsoids are drawn at the 30% probability level.

2.2. Biological evaluation

2.2.1. Cytotoxic activity of 3-hydroxy-3-pyrrolin-2-on derivates

In the first screening stage, cytotoxic activity of newly synthesized compounds (**D1**-**D15**) against HeLa, MDA-MB 231 and MRC-5 was evaluated by MTT assay. Cells were treated with single dose (100 μM) concentration of tested compounds. Four compounds: **D10**, **D13**, **D14**, and **D15** that showed the highest cytotoxicity against malignant cells and the best selectivity towards normal cells, were selected for further experiments (Table S3).

Cytotoxic effect of compounds **D10**, **D13**, **D14**, and **D15** was further examined in a range of five concentrations on all three cell lines during 24 h and 48 h using MTT and SRB assays. The main difference between these two assays is that MTT measures metabolic activity, while SRB is based on measurement of cellular protein content and indirectly measures cell number, so we performed both tests to define whether tested compounds kill or affect metabolic activity of cells [30,31]. Generally, both MTT and SRB assay showed comparable values of cytotoxic effect for all tested compounds on all three designated cell lines. Results of both assays are presented in the form of comparative dose-response curves (Fig. 2).

Compounds **D10**, **D13**, **D14**, and **D15** showed the cytotoxic effect on subjected tumor cell lines, being more potent for HeLa, than for MDA-MB 231. Calculated IC_{50} values for MDA-MB 231 and non-transformed fibroblasts MRC-5 were above the highest concentration used in experiments (IC_{50} > 100 μM). It was shown that all treatments on HeLa cells induced growth inhibition activity in dose and time-dependent manner. HeLa cells were more susceptible to tested compounds with moderate cytotoxic activity. Compound **D13** exhibited the strongest cytotoxic effect after 48 h of exposure against HeLa cells with IC_{50} values of 40.9 ± 5.9 μM and 54.35 ± 8.56 μM for SRB and MTT assays, respectively (Table S4).

From the above mentioned analysis, it can be noticed that when R_1 is benzyloxy group, activity of the compounds has been significantly improved as can be seen for three compounds (**D13**, **D14**, and **D15**) containing this fragment. Another significant influence of the substituents at R_1 was not observed except in case **D10** (R_1 = Cl) where there is also improved antitumour activity, but to some lesser extent compered to compounds with benzyloxy group. Also, it was observed that the shift of the nitro group from *meta*- to *para*-position, as can be seen in compounds **D13** and **D14**, had some influence to the cell growth inhibition. Some better antitumor activity is achieved when NO_2 group is in *meta*-position, as observed for **D13** in both MTT and SRB assay. This different activity was also observed for some organic compounds in a recent study [32], and is most likely related to the steric effect of the compounds. Slight difference in the activity was observed in **D15**, when Cl is replaced in R_4, showing the positive change in antitumour activity compering to **D14**.

There is no large amount of data on the antitumor effects of these types of compounds in the literature. Several studies indicate that their biological activity depends on the modifications of the heterocyclic ring. The 3-hydroxy-pyrrolin-2-one derivatives exhibited antitumor activity *in vitro* on three mouse tumor cell lines hepatoma (MG-22A), melanoma (V16) and neuroblastoma (Neuro2A) [33]. *In vivo* studies have shown that some pyrrolin-2-one derivatives had genotoxic effects on the mouse bone marrow [34]. There are also data on the antitumor effects of some diaryl-3-pyrroline-2-on derivatives on human malignant cells, such as U-937 histiocytic lymphoma cells [35]. Almost no data are available on the mechanism of action of these organic compounds, as well as the type of cell death they induce, so we examined whether cytotoxicity induced by tested compounds was due to apoptosis or cell cycle arrest.

2.2.2. The mechanisms of cytotoxic activity

To determine the type of cell death induced by selected 3-hydroxy-3-pyrrolin-2-one derivatives, Annexin V-FITC/7-AAD assay was performed. Flow cytometric analysis showed that all tested compounds induced apoptosis in HeLa cells, while the percent of necrotic cells was negligible. Considering that apoptosis, as opposed to necrosis, does not induce inflammation and injury of surrounding tissue, agents that induce this type of cell death can be envisaged as potential antitumor drugs [36]. In accordance with the results of MTT and SRB assay, flow cytometry showed that treatment of MDA-MB cells with 100 μM concentration of all tested compounds resulted in the small percent of dead, predominantly apoptotic cells (Fig. 3).

Likewise, the effect of 3-hydroxy-3-pyrrolin-2-one derivates on autophagy was different in these cell lines. While in HeLa cells compounds **D13** and **D15** induced marked and compound **D10** moderate increases in the intensity of red fluorescence. Contrary, in MDA-MB 231 cells not only that compounds **D13** and **D15** had no influence on autophagy induction but compounds **D10** and **D14** even inhibited autophagy in certain extent (Fig. 4).

To find out the role which autophagy plays in 3-hydroxy-3-pyrrolin-2-one derivates derivatives-induced cytotoxicity, cells were cotreated with autophagy inhibitor chloroquine (CQ). Results showed opposite effect of compounds **D13** and **D15** in HeLa and MDA-MB 231 cells (Fig. 5). While in HeLa cells inhibition of autophagy enhanced apoptosis, in MDA-MB 231 cells resulted in the decrease of Annexin V-positive cells. In compounds **D10** and **D14**, treated both HeLa and MDA-MB 231 cells autophagy inhibition had no effect on the induction of apoptosis.

Dual role of autophagy, a catabolic process by which cells degrade and recycle their own constituents, is well documented. Autophagy was first described as a mechanism for cell survival that maintains normal cellular function under conditions of intra- and extracellular stresses. However, autophagy may also activate the apoptotic program and promote cell death. For this reason, agents targeting autophagy may serve as a therapeutic advantage [37]. Our results showed that in HeLa cells autophagy induced by **D13** and **D15** has a cytoprotective role, since its' inhibition enhanced apoptosis. In **D13** and **D15** treated MDA-MB 231 cells autophagy stayed on the basal level, therefore inhibition

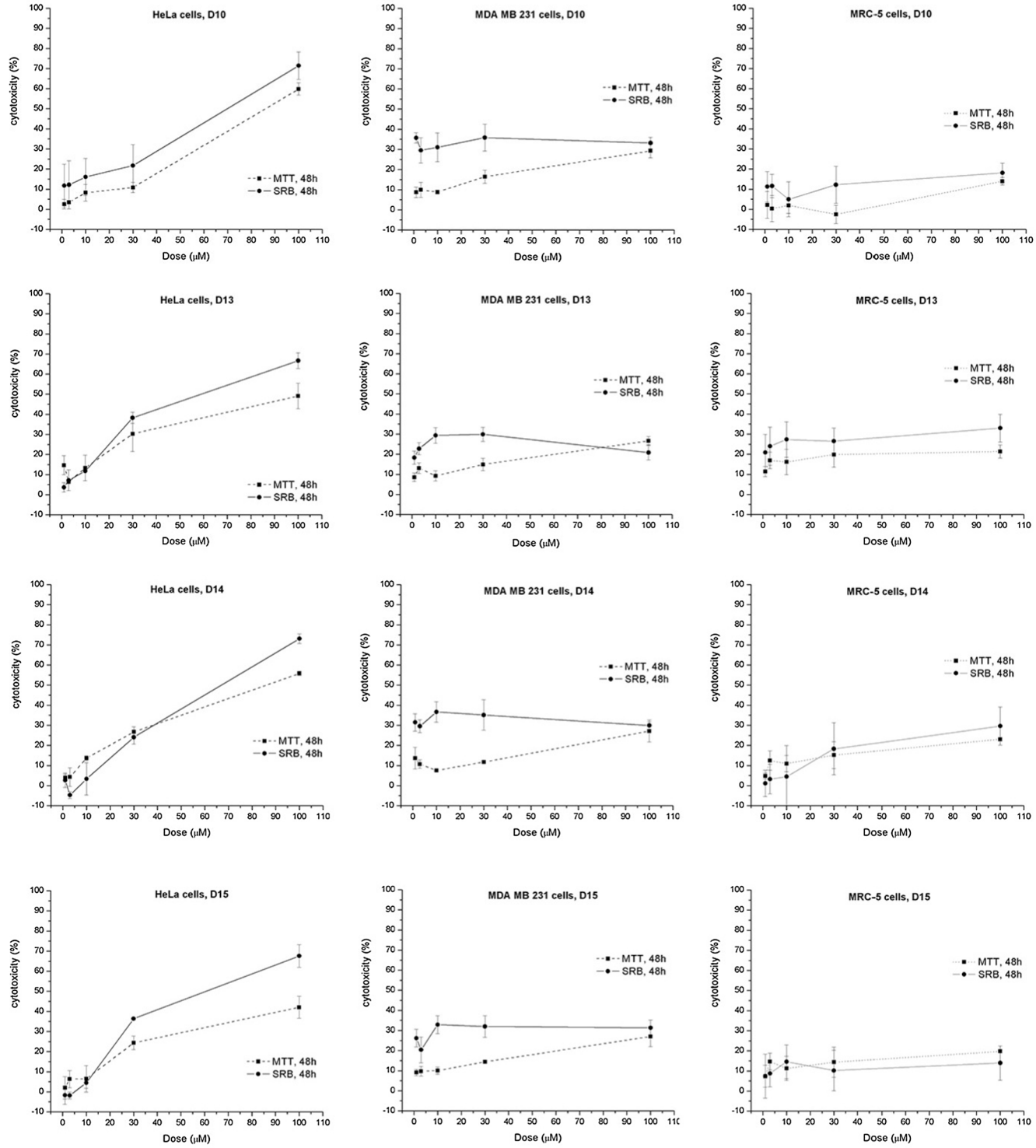

Fig. 2. Comparative dose-response curves of MTT and SRB assay after 48 h treatment of HeLa, MDA-MB 231 and MRC-5 with compounds **D10**, **D13**, **D14**, and **D15**. Results are presented as mean ± SD.

of autophagy, as a homeostatic mechanism, resulted in alleviation of cell death. Although compound **D10** enhanced autophagy in HeLa cells, cotreatment with CQ had no effect on apoptosis, showing that autophagy is not implicated in the cell death pathway. These results demonstrated that autophagy is not a part of the mechanisms of cytotoxicity induced by either tested 3-hydroxy-3-pyrrolin-2-one derivates.

To further reveal mechanisms underlying cytotoxicity induced by the tested compounds, cell cycle distribution was analyzed by flow cytometry. In multicellular organisms both apoptosis and process of cell cycle progression are essential for maintaining tissue homeostasis. Accumulated evidence revealed that these two processes share a set of regulatory molecules. Manipulation with cell cycle may prevent or induce apoptosis. Our results demonstrated that in HeLa cells treated with compounds **D13**, **D15** and **D10** arrested cells in S phase, indicating inhibition of DNA synthesis, while compound **D14** had no effect on cell cycle progression. As expected, 100 μM concentration of the 3-hydroxy-3-pyrrolin-2-one derivates didn't affect cell cycle progression in MDA-MB 231 cells (Fig. 6).

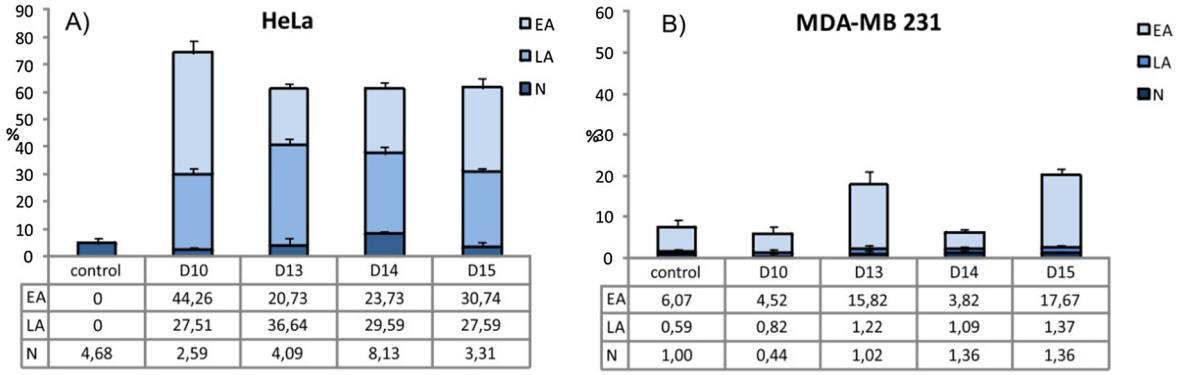

	control	D10	D13	D14	D15
EA	0	44,26	20,73	23,73	30,74
LA	0	27,51	36,64	29,59	27,59
N	4,68	2,59	4,09	8,13	3,31

	control	D10	D13	D14	D15
EA	6,07	4,52	15,82	3,82	17,67
LA	0,59	0,82	1,22	1,09	1,37
N	1,00	0,44	1,02	1,36	1,36

Fig. 3. Flow cytometric analysis of Annexin V-FITC/7-AAD staining. Graphs showing the percent of early apoptotic (EA), late apoptotic (LA) and necrotic cells (N) in untreated (control) and treated HeLa and MDA-MB 231 cells. Results are presented as average ± SD of three independent experiments.

In conclusion, HeLa and MDA-MB 231 cell lines differ not only in histological type, but are also highly heterogeneous regarding mutations related to genes that control programmed cell death and cell cycle progression. This fact explains the different sensitivity of these cell lines to the tested compounds. Tested compounds apparently target molecules that are diversely expressed in HeLa and MDA-MB 231 cells. The data presented suggest that selected 3-hydroxy-3-pyrrolin-2-one derivatives in HeLa cells induce apoptosis that is associated with S phase arrest (**D13**, **D15**, and **D10**) or unrelated to cell cycle distribution (**D14**).

2.3. Fluorescence measurements

2.3.1. Fluorescence quenching on EB–DNA

Ethidium bromide (EB) is compound known by intense fluorescence emission in the presence of DNA. Fluorescence emission, the consequence of strong intercalation between the base pairs of DNA and EB, can be quenched by the addition of the drug which can compete with EB to bind with DNA confirming that drug intercalates to base pairs of DNA [38,39]. Fluorescence quenching spectra (Fig. 7) of titration EB–DNA with **D13** and **D15**, recorded in the range of 550–750 nm, show a decreasing trend with the increasing amounts of the compounds at 610 nm indicating that EB was partially replaced by compounds **D13** and **D15**. The molar ratios of EB-DNA : **D13** or **D15** followed the order: 1 : 0 (control), 1 : 0.2, 1 : 0.4, 1 : 0.6, 1 : 0.8, 1 : 1, 1 : 1.2, 1 : 1.4, 1 : 1.6, 1 : 8, 1 : 2, in a total volume of 5.0 ml, pH 7.4, at 25 °C with an incubation time of 6 h. Obtained results indicated that both compounds bind to DNA by an intercalative mode.

To better understand quantitatively the magnitude of the binding strength of the compounds with CT-DNA, the quenching constant (Kq) was calculated using Sterne-Volmer equation [40] by examining the dependence of F_0/F on [Q] (Fig. 7). Quenching constant for **D13** and **D15**, presented in Table 1, indicate that both compounds have the capability to displaced EB from the EB–DNA complex by binding to DNA through intercalation [41].

2.3.2. Protein binding experiments

Based on the fact that the efficiency of drugs depends on their ability to bind to a carrier protein and knowing that bovine serum albumin (BSA) is the protein that has the ability to transport drugs in bloodstream we investigated the binding affinity of **D13** and **D15** to BSA. In the fluorescence quenching experiment, the fluorescence emission titration of BSA with compounds **D13** and **D15** was used for the investigation of binding properties by increasing the concentration of the quenchers, in the wavelength range of 300–500 nm (Fig. 8).

The molar ratios of BSA : **D13** or **D15** followed the order: 1 : 0 (control), 1 : 1, 1 : 2, 1 : 3, 1 : 4, 1 : 5, 1 : 6, 1 : 7, 1 : 8, 1 : 9, 1 : 10, in total volume of 5.0 ml, pH 7.4, at 25 °C with the incubation time of 6 h. The fluorescence quenching data such as binding constant (K_a) and number of binding sites per BSA molecule (n) were described by using Eqn [42]:

$$\log(F_0 - F/F) = \log K_a + n \log[Q]$$

where F_0 is the emission intensity in the absence of a quencher, F is the emission intensity in the presence of a quencher for the complexes **D13** or **D15**–BSA and [Q] is the concentration of **D13** or **D15**. The K_a value and n were obtained investigating dependence of the log $[(F_0–F)/F]$ versus log[Q] (Fig. 8). The obtained values of the K_a, given in Table 2, that are in the optimum range which is considered to be 10^4–10^6 M^{-1} [43], indicate that both compounds have the appropriate ability for binding to BSA. The number of binding sites of **D13** or **D15** ($n \approx 1.5$, Table 2) point that both **D13** and **D15** bind to BSA in the molar ratio of 1.5 : 1.

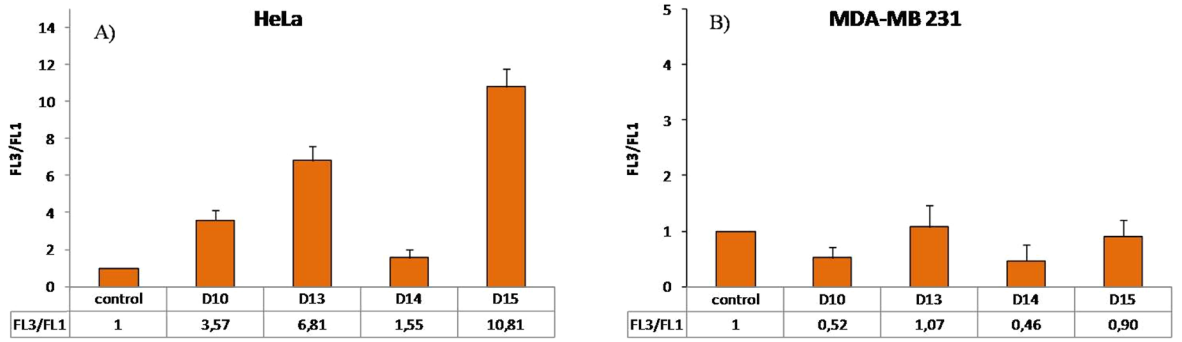

	control	D10	D13	D14	D15
FL3/FL1	1	3,57	6,81	1,55	10,81

	control	D10	D13	D14	D15
FL3/FL1	1	0,52	1,07	0,46	0,90

Fig. 4. Quantification of autophagy. Graphs showing the change in red/green (FL3/FL1) mean fluorescence intensity in untreated (control) and treated HeLa and MDA-MB 231 cells. Results are presented as average ± SD from three independent experiments.

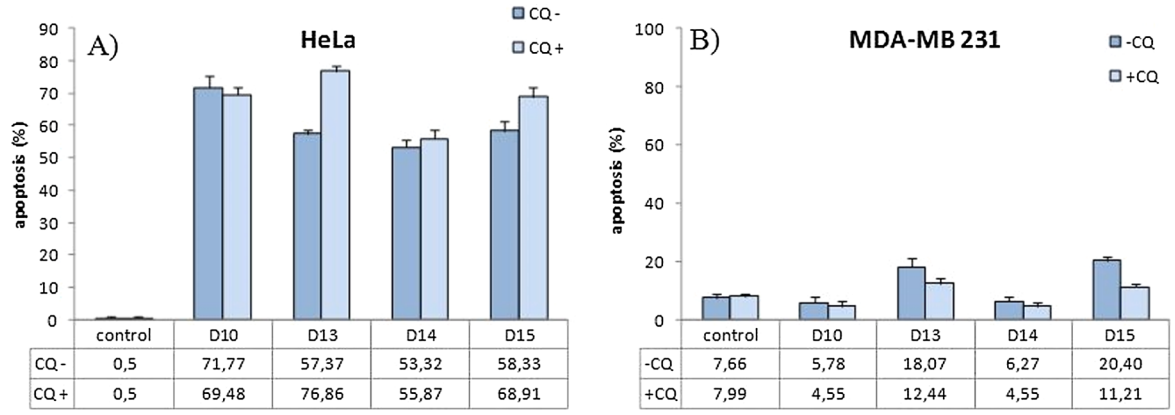

	control	D10	D13	D14	D15
CQ-	0,5	71,77	57,37	53,32	58,33
CQ+	0,5	69,48	76,86	55,87	68,91

	control	D10	D13	D14	D15
-CQ	7,66	5,78	18,07	6,27	20,40
+CQ	7,99	4,55	12,44	4,55	11,21

Fig. 5. Influence of autophagy inhibition on apoptosis. Percent of apoptotic cells with (CQ+) or without (CQ−) cotreatment with autophagy inhibitor chloroquine determined by flow cytometric analysis of Annexin V/7-AAD double stained cells. Results are presented as average ± SD from three independent experiments.

2.4. Viscosity measurements

The viscosity measurement of DNA after treatment with a varying concentration of ligands provides a reliable indication for the DNA binding mode. In general, this technique provides more definitive evidence for intercalative binding of particular substances to DNA, since changes in the DNA chain length are manifested by changes in the viscosity of the medium.

It is generally suggested that a classical intercalative binding mode causes a significant increase of DNA viscosity because the intercalative interaction requires the space of adjacent base pairs to be large enough to accommodate the bound small molecules and elongates the double helix. When electrostatic, groove or hydrophobic binding occurs in the binding process, no obvious changes of DNA viscosity are typically caused in the solution.

The relative specific viscosity (η/η_o) of DNA is firmly dependent on the length changes that may associate with the separation of DNA base pairs caused by intercalative interaction between DNA's double helix and a small molecule. The influences of investigated ligands **D13** and **D15** on the viscosity of DNA are shown in Fig. 9. In our case, relative viscosity increase with a slope value of 0.52 (ligand **D13**) and 0.55 (ligand **D15**).

Upon addition of both ligands to DNA, the relative viscosity raises steadily, as in the case of the classical intercalator. The results indicated that the ligands bind with DNA through the intercalative mode since the viscosity increase of DNA is ascribed to the intercalative binding mode, causing the effective lengthening of the DNA. The slope of relative viscosity was similar for both ligands, pointing out to similar binding affinity towards DNA for investigated compounds.

2.5. DNA and BSA docking study

The method of molecule simulation is an efficient way to determine and predict the binding mode and the interaction region. To elucidate the mode of interaction and binding affinity, docking studies have been performed on B-DNA and BSA in presence of **D13, D14** and **D15**. The best-docked poses of the compounds with DNA dodecamer are displayed in Fig. 10, and calculated results for binding energies and docked inhibition constant are summarised in Table 3. The study revealed that ligands under investigation interact with DNA *via* an intercalation mode involving outside edge π–π stacking interactions between guanine and benzyl ring of the ligands. From the ensuing docked structures it is clear that all ligands fits well into the minor groove of the targeted DNA and it is mainly stabilized by van der Waals interaction as can be seen from Fig. 10. The relative binding energy of the docked structures was found to be −51.035, −49.814 and −52.312 kJ mol^{-1} for **D13, D14** and **D15** respectively. The slightly lower binding energy for **D14** can be consequence of one less electrostatic interaction of $-NO_2$ group. From Fig. 10 it can be noted the different orientation of **D13** and **D14** towards DNA during docking, compared to **D15**. Namely, for **D13** and **D14** docking is additionally stabilized by electrostatic interactions between $-NO_2$ and adenine, which cause different conformation after docking in contrast to **D15**. On the other hand, chlorobenzyl ring for **D15** is outside of DNA helixes and not contribute to the binding affinity of ligand. The slightly higher binding energy for **D15** can be attributed to one more π–π stacking interaction of the ligand with DNA.

The binding of ligands **D13, D14** and **D15** to BSA occurs at similar positions in domain I [44]. The essential driving force of **D13, D14** and **D15** binding to BSA is hydrophobic and a van der Waals force. Three hydrogen bonds have been observed in the **D13**-BSA system: oxygens

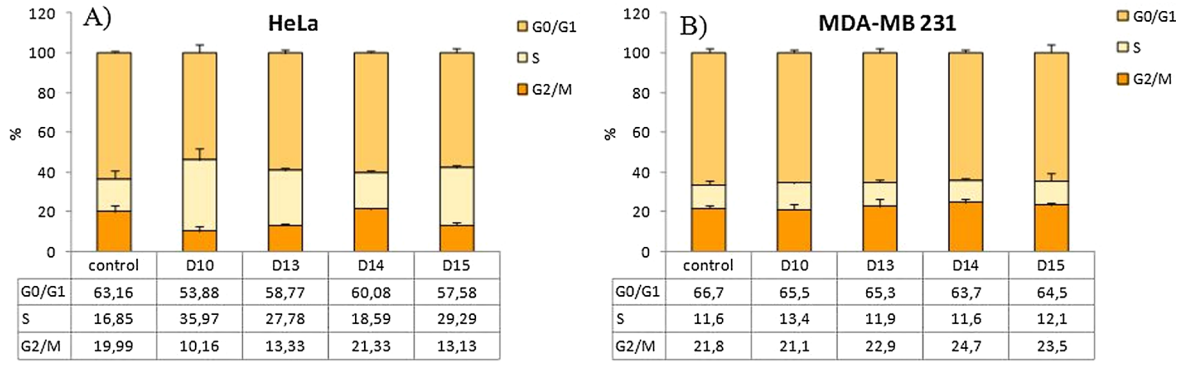

	control	D10	D13	D14	D15
G0/G1	63,16	53,88	58,77	60,08	57,58
S	16,85	35,97	27,78	18,59	29,29
G2/M	19,99	10,16	13,33	21,33	13,13

	control	D10	D13	D14	D15
G0/G1	66,7	65,5	65,3	63,7	64,5
S	11,6	13,4	11,9	11,6	12,1
G2/M	21,8	21,1	22,9	24,7	23,5

Fig. 6. Cell cycle analysis. Graphs showing cell cycle distribution in untreated (control) and treated HeLa and MDA-MB cells. Results are presented as average ± SD of three independent experiments.

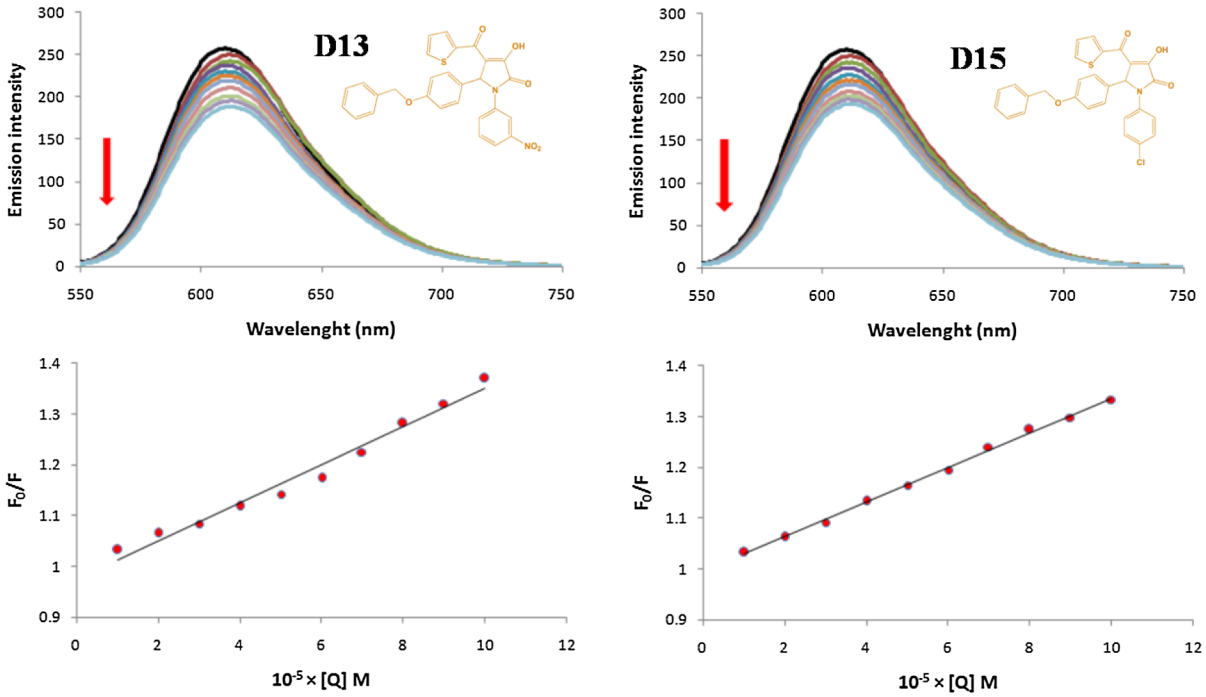

Fig. 7. Top: Emission spectra of EB-DNA in the absence (black lines) and in the presence of compounds **D13** and **D15**. [EB] = 50 μM, [DNA] = 50 μM; [**D13**] and [**D15**] = 0–100 μM; pH = 7.4; λ_{ex} = 500 nm. Bottom: Plots of F_0/F versus [Q].

Table 1
The bimolecular quenching rate constant (k_q), Stern–Volmer constant (K_{sv}), and correlation coefficient (R) for compounds **D13** and **D15**.

Compound	k_q [M^{-1} s^{-1}]	K_{sv} [M^{-1}]	R
D13	(3.7 ± 0.1) × 10^{11}	(3.7 ± 0.1) × 10^3	0.989
D15	(3.4 ± 0.1) × 10^{11}	(3.4 ± 0.1) × 10^3	0.998

Table 2
Binding parameters (K_a and n) and the correlation coefficient (R) for interactions of **D13** and **D15** with BSA.

Compound	K_a [M^{-1}]	n	R
D13	(4.2 ± 0.2) × 10^5	1.47	0.998
D15	(2.6 ± 0.2) × 10^5	1.69	0.998

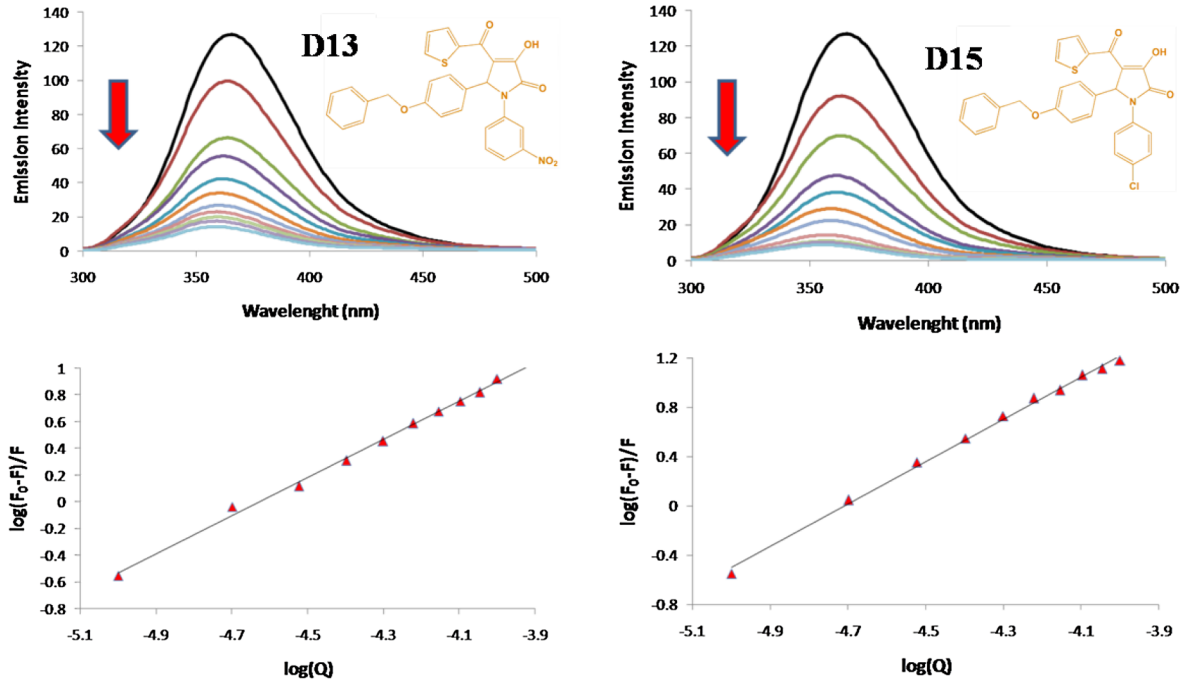

Fig. 8. Top: emission spectra of BSA in the absence (black lines) and in the presence of compounds **D13** and **D15**. [BSA] = 10.0 μM; [**D13**] or [**D15**] = 0, 10, 20, 30, 40, 50, 60, 70, 80, 90 and 100 μM; pH = 7.4; λ_{ex} = 280 nm. Bottom: plots of $\log(F_0\text{-}F/F)$ versus log[Q].

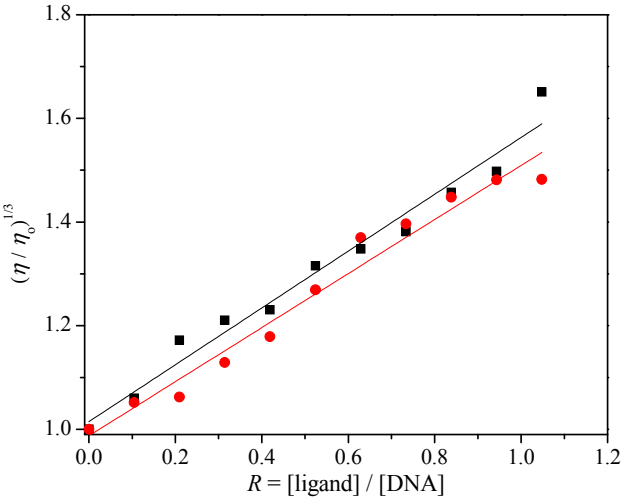

Fig. 9. Relative viscosity $(\eta/\eta_o)^{1/3}$ of DNA (0.01 mM) in buffer solution (50 mM NaCl and 5 mM Tris-HCl at pH 7.4) in the presence of the complex **D15** (black square) and **D13** (red circle) at increasing amounts (*R*). Solid lines represent the fitted linear regression curve.

from $-NO_2$ group makes two hydrogen bonds with Lys A:136 and Phe A:36 and one is formed between oxygen (from benzyloxy fragment) and Phe B:36. For ligand **D14** interaction with BSA occurs *via* 4 hydrogen bonds, three the same like in **D13**, and one additional between −OH group and Lys B:136. In the case of **D15**, only one hydrogen bond is formed with Glu A:38 (Fig. 11). The formation of hydrogen bonds stabilizes the complexes of **D13** and **D14** with BSA significantly more than **D15**-BSA which is demonstrated by higher binding energy for **D13** and **D14**. The interactions of all ligands were additionally intensified by π–π stacking interactions with Lys amino acids (Lys B:132 and Lys B:136). Because the binding site is located deeply in the body of BSA instead of being on the surface of the protein, both ligands have to pass through the amino acid residues on the surface around the binding site to settle at the proper position in BSA. This process is against the binding process and increases the activation energy of the binding.

3. Conclusion

The three-component reaction between acylpyruvic acid ethyl ester and a mixture of differently substituted aromatic aldehyde and an aromatic amine, in glacial acetic acid as catalyst and solvent, is used for synthesis of fifteen 1,5-diaryl-4-(2-thienylcarbonyl)-3-hydroxy-3-pyrrolin-2-ones (**D1**-**D15**), fourteen novel and one previously reported. All synthesized compounds were characterized by UV–Vis, NMR, MS spectroscopy and elemental analysis. In addition, for compound **D2**, crystallized from DMSO solution, crystal structure was determined using single-crystal X-ray diffraction analysis. All the compounds were further tested for their cytotoxic effect on human cancer cell lines HeLa and MDA-MB 231 and normal fibroblasts (MRC-5). Compounds **D10**, **D13**, **D14**, and **D15** showed cytotoxic effect on subjected tumor cell lines, being more potent for HeLa than for MDA-MB 231, but **D13** exhibited the strongest cytotoxic effect after 48 h of exposure against HeLa cells with IC_{50} values of 40.9 ± 5.9 μM and 54.35 ± 8.56 μM for SRB and MTT assays, respectively. All four compounds that showed the highest cytotoxicity against malignant cells and the best selectivity towards normal cells were placed under further experiments. Results obtained by investigating mechanisms of cytotoxic activity suggest that our tested compounds in HeLa cells induce apoptosis that is associated with S phase arrest (compounds **D13**, **D15**, and **D10**) or unrelated to cell cycle distribution (compound **D14**). In order to better understand their appropriateness for potential use as anticancer medicaments we studied the interactions between biomacromolecules (DNA or BSA) and **D13** and **D15**. The obtained results indicated that **D13** and **D15** have great affinity to displace EB from the EB-DNA complex through intercalation [K_{sv} = (3.7 ± 0.1) and (3.4 ± 0.1) × 10^3 M^{-1}, respectively] that is also confirmed *via* viscosity measurements experiments. K_a values, obtained as result of fluorescence titration of BSA with **D13** and **D15** [K_a = (4.2 ± 0.2) and (2.6 ± 0.2) × 10^5 M, respectively], showed that a significant amount of the tested compounds could be transported and distributed through the cells. In addition, DNA and BSA molecular docking study for **D13, D14** and **D15** was further performed to elucidate the mode of interaction and binding affinity.

4. Experimental section

4.1. Materials

All solvents and substrate were purchased from Sigma. The (Z)-ethyl 2-hydroxy-4-oxo-4-(thiophen-2-yl)but-2-enoate (**A**) was synthesized according to the previously described methodology [45]. Melting-points (Mp) were determined on a Mel-Temp apparatus and are uncorrected. Thin-layer chromatography (TLC) was carried out on 0.25 mm Sigma-Aldrich coated silica gel plates (60F-254) using eluent DCM : EtOH (9:1) as a mobile phase and UV light for visualization. The IR spectra were recorded by a Perkin–Elmer Spectrum One FT-IR spectrometer on KBr pellet. The NMR spectra of **D1-D15** were performed in DMSO-d_6 with TMS as internal standard on a Varian Gemini 200 MHz NMR spectrometer (^{1}H at 200 and ^{13}C at 50 MHz). Mass spectrometry was performed by Waters Micromass Quattro II triple quadrupole mass spectrometer and MassLynx software for control and data processing, electrospray ionization in the positive mode was used. The electrospray capillary was set at 3.0 kV and the cone at 20 V, the ion source temperature was set at 120 °C and the flow rates for nitrogen bath and spray were 500 l/h and 50 l/h, respectively and the collision energy was 20 eV.

4.2. General procedure for synthesis of 1,5-diaryl-4-(2-thienylcarbonyl)-3-hydroxy-3-pyrrolin-2-ones

A mixture of 1 mmol of an aromatic aldehyde and 1 mmol of an aromatic amine dissolved in 3 ml of glacial acetic acid was heated to 50 °C. After reaching the temperature, 1 mmol of the (*Z*)-ethyl 2-hydroxy-4-oxo-4-(thiophen-2-yl)but-2-enoate, dissolved in 2 ml glacial acetic acid, was added dropwise. After 3–5 h of reaction time precipitation of the product occurred. The reaction is followed by thin-layer chromatography with CH_2Cl_2 : CH_3CH_2OH = 9 : 1 as the eluent. After 8 h of reaction time mixture was cooled, the precipitate was filtered off, washed with anhydrous diethyl ether, and dried at the room temperature to yield. All the synthesized compounds were characterized by NMR spectroscopy (^{1}H and ^{13}C spectra are presented in the ESI, Figs. S1–S30).

4.2.1. 3-Hydroxy-5-phenyl-1-(o-tolyl)-4-(2-thienylcarbonyl)-2,5-dihydro-1H-pyrrol-2-one (D1)

White powder; yield: 85%; mp = 257 °C; IR (KBr): ν 3246, 1710, 1690, 1680, 1612, 1515, 1499, 1405, 1339, 1299, 1248, 1184, 1053, 988, 856, 832, 762, 740 cm^{-1}; ^{1}H NMR (200 MHz, DMSO-d_6): δ = 1.91 (s, 3H, CH_3), 6.44 (s, 1H, CH), 7.03–7.30 (m, 4H, CH_{Ar}), 7.38–7.43 (m, 2H, CH_{Ar}), 7.88–8.09 (m, 4H, CH_{Ar}), 8.11–8.25 (m, 2H, CH_{Ar}) ppm; ^{13}C NMR (50 MHz, DMSO-d_6): δ = 21.2, 61.2, 121.2, 121.9, 124.5, 127.9, 128.4, 128.7, 134.9, 135.6, 135.9, 143.3, 143.7, 143.9, 148.2, 165.5, 172.2 and 180.5 ppm; ESI-MS: *m/z* (%) = 375 $[M]^+$. Calcd for $C_{22}H_{17}NO_3S$ (%): C 70.38, H 4.56, N 3.73; found: C 70.52, H 4.51, N 3.75.

4.2.2. 3-Hydroxy-5-phenyl-1-(p-tolyl)-4-(2-thienylcarbonyl)-2,5-dihydro-1H-pyrrol-2-one (D2)

White powder; yield: 88%; ^{1}H NMR (200 MHz, DMSO-d_6): δ = 1.91 (s, 3H, CH_3), 6.24 (s, 1H, CH), 6.99–7.38 (m, 8H, CH_{Ar}), 7.47 (d, 2H,

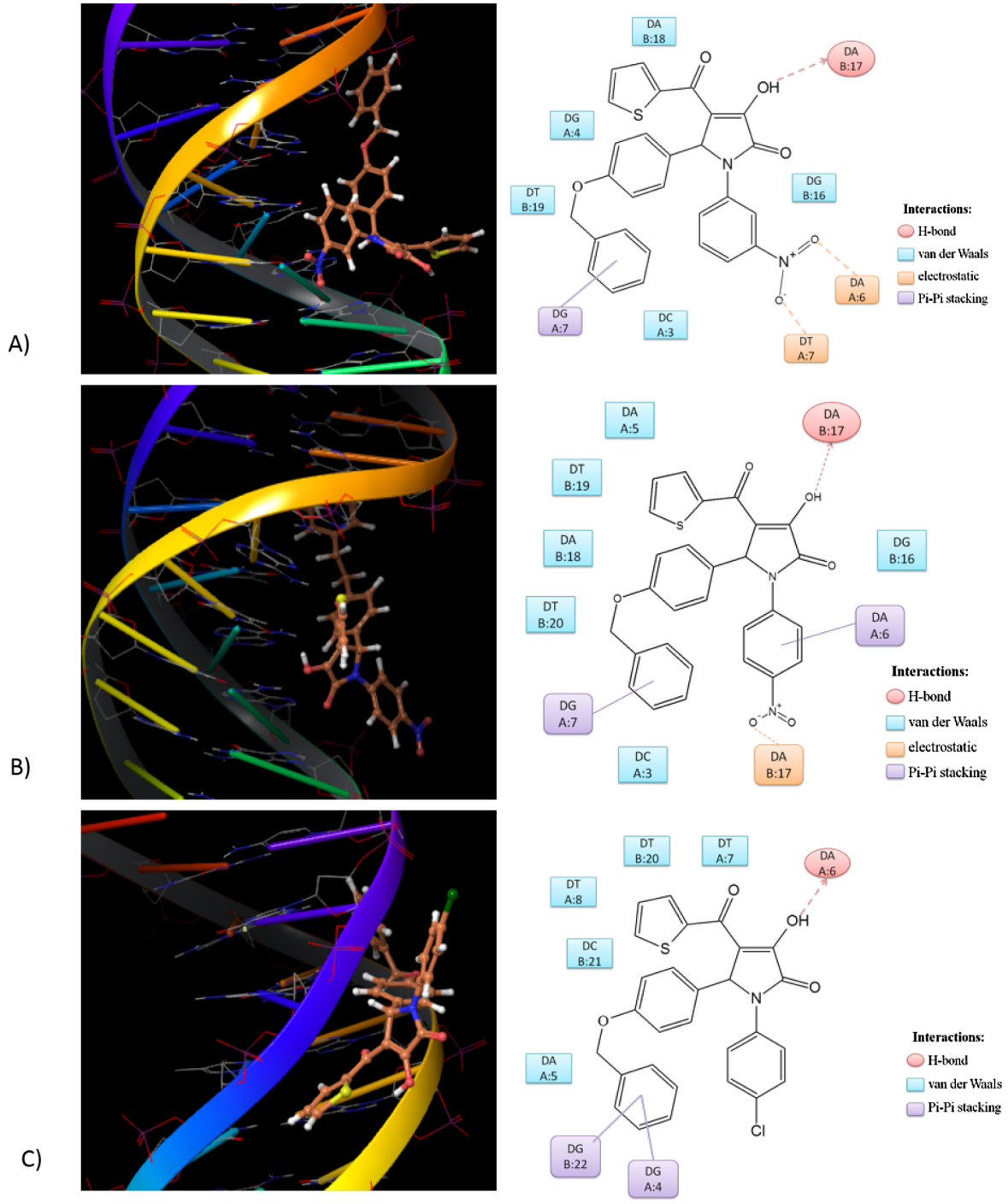

Fig. 10. Molecular docking of **D13** (A), **D14** (B) and **D15** (C) with DNA and a two-dimensional representation of interactions.

Table 3
Docking parameters of **D13, D14** and **D15.**

Compound	Docking score	Binding energy/kJ·mol^{-1}	Docking inhibition constant μM
		DNA	
D13	−4.852	−51.035	1.144
D14	−4.551	−49.814	1.873
D15	−5.187	−52.312	0.684
		BSA	
D13	−4.075	−55.203	0.213
D14	−3.848	−57.662	0.079
D15	−4.253	−51.643	0.895

J = 8.4 Hz, CH_{Ar}), 7.95 (dd, 1H, J = 4.9, 1.1 Hz), 8.05 (dd, 1H, J = 3.8, 1.1 Hz) ppm; ^{13}C NMR (50 MHz, DMSO-d_6): δ = 20.6, 21.2, 61.6, 120.2, 122.9, 127.9, 128.1, 128.5, 128.6, 129.3, 133.9, 134.6, 134.9, 135.2, 136.5, 144.1, 149.3 and 164.5 ppm; ESI-MS: m/z (%) = 375 $[M]^+$. Calcd for $C_{22}H_{17}NO_3S$ (%): C 70.38, H 4.56, N 3.73; found: C 70.52, H 4.51, N 3.75.

4.2.3. 3-Hydroxy-5-phenyl-1-(4-hydroxyphenyl)-4-(2-thienylcarbonyl)-2,5-dihydro-1H-pyrrol-2-one ***(D3)***

Yellow powder; yield: 72%; mp = 246 °C; IR (KBr): ν 3468, 3199, 1701, 1677, 1610, 1520, 1455, 1409, 1376, 1262, 1239, 1181, 1137, 1125, 996, 836, 824, 740, 714 cm^{-1}; ^{1}H NMR (200 MHz, DMSO-d_6): δ = 6.16 (s, 1H, CH), 6.61–6.74 (m, 2H, CH_{Ar}), 7.07–7.39 (m, 8H,

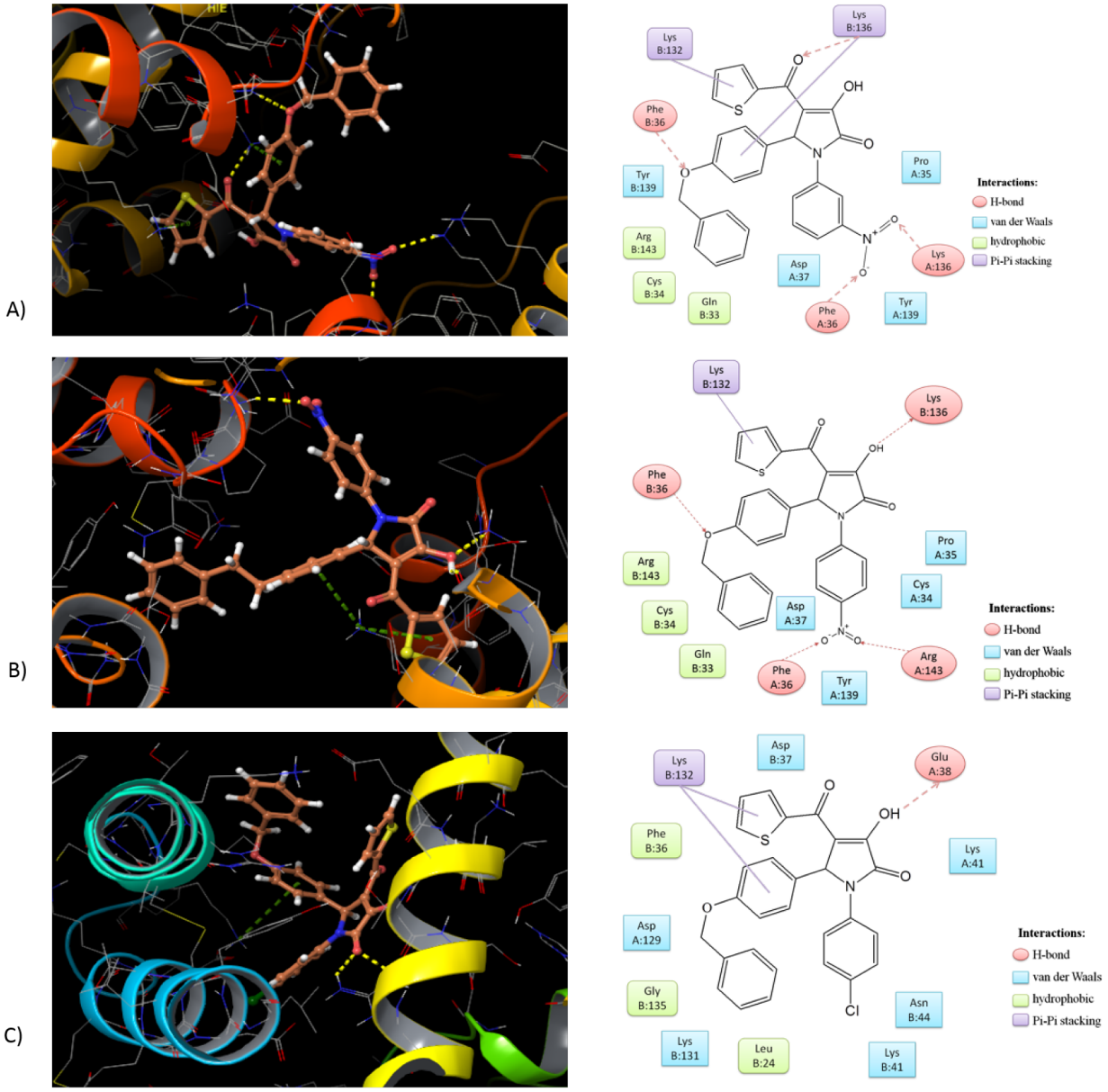

Fig. 11. Molecular docking of **D13** (A), **D14** (B) and **D15** (C) with BSA and a two-dimensional representation of interactions.

CH_{Ar}), 7.95 (dd, 1H, J = 4.9 Hz, 1.1 CH_{Ar}), 8.06 (dd, 1H, J = 3.8, 1.1 Hz), 9.47 (s, 1H, OH_{Ar}) ppm; ^{13}C NMR (50 MHz, DMSO-d_6): δ = 115.4, 119.9, 125.0, 127.8, 127.9, 128.5, 128.6, 136.6, 144.2, 149.6, 155.4, 164.3 and 180.4 ppm; ESI-MS: m/z (%) = 377 $[M]^+$. Calcd for $C_{21}H_{15}NO_4S$ (%): C 66.83, H 4.01, N 3.71; found: C 67.01, H 4.11, N 3.75.

*4.2.4. 3-Hydroxy-5-phenyl-1-(4-chorophenyl)-4-(2-thienylcarbonyl)-2,5-dihydro-1H-pyrrol-2-one **(D4)***

White powder; yield: 81%; mp = 240 °C; IR (KBr): ν 3187, 1709, 1672, 1610, 1495, 1414, 1370, 1298, 1281, 1245, 1187, 1091, 987, 852, 836, 742, 725 cm^{-1}; ^{1}H NMR (200 MHz, DMSO-d_6): δ = 6.32 (s, 1H, CH), 7.09–7.24 (m, 4H, CH_{Ar}), 7.29–7.42 (m, 4H, CH_{Ar}), 7.61–7.70 (m, 2H, CH_{Ar}), 7.96 (dd, 1H, J = 4.9 Hz, 1.1 CH_{Ar}), 8.02 (dd, 1H, J = 3.8, 1.1 Hz), 12.0 (s, 1H, OH_{enol}) ppm; ^{13}C NMR (50 MHz, DMSO-d_6): δ = 61.4, 120.5, 124.3, 127.9, 128.6, 128.8, 129.6, 135.4, 136.2, 144.0, 148.9, 164.8 and 180.4 ppm; ESI-MS: m/z (%) = 396 $[M]^+$. Calcd for $C_{21}H_{14}ClNO_3S$ (%): C 63.72, H 3.56, N 3.54; found: C 63.52, H 3.59, N 3.55.

*4.2.5. 3-Hydroxy-5-phenyl-1-(4-bromophenyl)-4-(2-thienylcarbonyl)-2,5-dihydro-1H-pyrrol-2-one **(D5)***

White powder; yield: 84%; mp = 237 °C; IR (KBr): ν 3188, 1709, 1684, 1671, 1610, 1492, 1412, 1370, 1297, 1245, 1128, 986, 852, 833, 741, 724 cm^{-1}; ^{1}H NMR (200 MHz, DMSO-d_6): δ = 6.31 (s, 1H, CH), 7.02–7.41 (m, 6H, CH_{Ar}), 7.41–7.68 (m, 4H, CH_{Ar}), 7.96 (dd, 1H, J = 5.0 Hz, 1.1 CH_{Ar}), 8.05 (dd, 1H, J = 3.8, 1.2 Hz) ppm; ^{13}C NMR (50 MHz, DMSO-d_6): δ = 117.9, 120.5, 124.6, 127.9, 128.6, 131.7, 135.8, 136.2, 144.0, 148.9, 165.8 and 180.4 ppm; ESI-MS: m/z (%) = 440 $[M]^+$. Calcd for $C_{21}H_{14}BrNO_3S$ (%): C 57.28, H 3.20, N 3.18; found: C 57.42, H 3.22, N 3.15.

*4.2.6. 3-Hydroxy-5-phenyl-1-(4-iodophenyl)-4-(2-thienylcarbonyl)-2,5-dihydro-1H-pyrrol-2-one **(D6)***

White powder; yield: 72%; mp = 239 °C; IR (KBr): ν 3178, 1684, 1665, 1608, 1490, 1413, 1383, 1292, 1244, 1134, 983, 852, 826, 715, 698 cm^{-1}; ^{1}H NMR (200 MHz, DMSO-d_6): δ = 6.30 (s, 1H, CH), 7.09–7.24 (m, 4H, CH_{Ar}), 7.30–7.35 (m, 2H, CH_{Ar}), 7.41–7.51 (m, 2H, CH_{Ar}), 7.59–7.69 (m, 2H, CH_{Ar}), 7.96 (dd, 1H, J = 5.0 Hz, 1.1 CH_{Ar}), 8.04 (dd, 1H, J = 3.8, 1.2 Hz) ppm; ^{13}C NMR (50 MHz, DMSO-d_6):

δ = 61.2, 90.3, 120.5, 124.7, 127.8, 128.2, 128.6, 134.7, 135.3, 136.2, 137.5, 144.0, 148.8, 165.7 and 180.4 ppm; ESI-MS: *m/z* (%) = 487 $[M]^+$. Calcd for $C_{21}H_{14}INO_3S$ (%): C 51.76, H 2.90, N 2.87; found: C 51.86, H 2.91, N 2.85.

4.2.7. 3-Hydroxy-1-(4-chorophenyl)-4-(2-thienylcarbonyl)-5-(4-nitrophenyl)-2,5-dihydro-1H-pyrrol-2-one (D7)

Yellow powder; yield: 77%; mp = 225 °C; IR (KBr): ν 3102, 1703, 1667, 1599, 1535, 1494, 1411, 1376, 1350, 1264, 1244, 1205, 1092, 987, 836, 745, 728 cm^{-1}; ^1H NMR (200 MHz, DMSO-d_6): δ = 6.50 (s, 1H, CH), 7.14–7.29 (m, 1H, CH_{Ar}), 7.37 (d, 2H, *J* = 8.8 Hz, CH_{Ar}), 7.65–7.70 (m, 4H, CH_{Ar}), 7.87–8.18 (m, 4H, CH_{Ar}) ppm; ^{13}C NMR (50 MHz, DMSO-d_6): δ = 21.2, 60.6, 119.4, 123.6, 124.2, 128.6, 128.9, 129.3, 129.9, 134.6, 135.0, 135.3, 143.8, 144.2, 147.3, 149.7, 164.6 and 179.9 ppm; ESI-MS: *m/z* (%) = 441 $[M]^+$. Calcd for $C_{21}H_{13}ClN_2O_5S$ (%): C 57.21, H 2.97, N 6.35; found: C 57.42, H 3.00, N 6.32.

4.2.8. 3-Hydroxy-1-(4-bromophenyl)-4-(2-thienylcarbonyl)-5-(4-nitrophenyl)-2,5-dihydro-1H-pyrrol-2-one (D8)

Yellow powder; yield: 79%; mp = 188 °C; IR (KBr): ν 3084, 1702, 1667, 1599, 1534, 1489, 1410, 1375, 1349, 1264, 1243, 1197, 1130, 986, 834, 745, 728 cm^{-1}; ^1H NMR (200 MHz, DMSO-d_6): δ = 6.49 (s, 1H, CH), 7.21 (dd, 1H, *J* = 4.9, 3.9 Hz, CH_{Ar}), 7.50 (d, 2H, *J* = 8.9 Hz, CH_{Ar}), 7.57–7.73 (m, 4H, CH_{Ar}), 7.90–8.18 (m, 4H, CH_{Ar}) ppm; ^{13}C NMR (50 MHz, DMSO-d_6): δ = 21.2, 60.5, 118.1, 119.3, 123.6, 124.5, 128.6, 129.3, 131.8, 134.6, 135.3, 135.4, 143.8, 144.3, 147.3, 149.8, 164.6 and 179.8 ppm; ESI-MS: *m/z* (%) = 485 $[M]^+$. Calcd for $C_{21}H_{13}BrN_2O_5S$ (%): C 51.97, H 2.70, N 5.77; found: C 52.02, H 2.71, N 5.75.

4.2.9. 3-Hydroxy-1-(4-iodophenyl)-4-(2-thienylcarbonyl)-5-(4-nitrophenyl)-2,5-dihydro-1H-pyrrol-2-one (D9)

Yellow powder; yield: 67%; mp = 195 °C; IR (KBr): ν 3106, 1710, 1669, 1602, 1518, 1490, 1410, 1373, 1346, 1267, 1245, 1193, 1129, 1056, 986, 827, 743, 720 cm^{-1}; ^1H NMR (200 MHz, DMSO-d_6): δ = 6.49 (s, 1H, CH), 6.47–6.50 (m, 1H, CH), 7.15–7.27 (m, 1H, CH), 7.47 (d, 2H, *J* = 8.8 Hz), 7.60–7.72 (m, 4H, CH_{Ar}), 7.95–8.12 (m, 4H, CH_{Ar}) ppm; ^{13}C NMR (50 MHz, DMSO-d_6): δ = 21.2, 60.4, 90.7, 119.3, 123.6, 124.5, 128.6, 129.3, 134.6, 135.3, 135.9, 137.7, 143.8, 144.3, 147.3, 149.9, 164.6 and 179.8 ppm; ESI-MS: *m/z* (%) = 532 $[M]^+$. Calcd for $C_{21}H_{13}IN_2O_5S$ (%): C 47.38, H 2.46, N 5.26; found: C 47.30, H 2.44, N 5.28.

4.2.10. 3-Hydroxy-1-(p-tolyl)-4-(2-thienylcarbonyl)-5-(4-chlorophenyl)-2,5-dihydro-1H-pyrrol-2-one (D10)

Yellow powder; yield: 92%; mp = 240 °C; IR (KBr): ν 3099, 1708, 1666, 1595, 1513, 1407, 1379, 1268, 1245, 1089, 988, 826, 751, 729 cm^{-1}; ^1H NMR (200 MHz, DMSO-d_6): δ = 1.91 (s, 3H, CH_3), 6.28 (s, 1H, CH), 7.10 (d, 2H, *J* = 8.3 Hz), 7.16–7.28 (m, 3H, CH), 7.35 (d, 2H, *J* = 8.5 Hz), 7.47 (d, 2H, *J* = 8.4 Hz), 7.96 (dd, 1H, *J* = 4.9, 1.0 Hz), 8.08 (dd, 2H, *J* = 3.8, 1.0 Hz) ppm; ^{13}C NMR (50 MHz, DMSO-d_6): δ = 20.6, 21.2, 60.8, 119.6, 122.8, 128.4, 128.6, 129.3, 129.7, 132.6, 133.6, 134.5, 135.0, 135.2, 135.7, 144.0, 149.5, 164.3 and 180.2 ppm; ESI-MS: *m/z* (%) = 410 $[M]^+$. Calcd for $C_{22}H_{16}ClNO_3S$ (%): C 64.47, H 3.93, N 3.42; found: C 64.53, H 3.91, N 3.40.

4.2.11. 3-Hydroxy-1,5-bis(4-chlorophenyl)-4-(2-thienylcarbonyl)-2,5-dihydro-1H-pyrrol-2-one (D11)

White powder; yield: 85%; mp = 231 °C; IR (KBr): ν 3172, 1711, 1670, 1607, 1494, 1416, 1371, 1280, 1248, 1090, 988, 833, 760, 724 cm^{-1}; ^1H NMR (200 MHz, DMSO-d_6): δ = 6.34 (s, 1H, CH), 7.19–7.28 (m, 3H, CH), 7.34–7.43 (m, 4H, CH), 7.66 (d, 2H, *J* = 9.0 Hz), 7.97 (dd, 1H, *J* = 4.9, 1.1 Hz), 8.09 (dd, 1H, *J* = 3.8, 1.1 Hz), 11.87 (br. s, 1H, OH_{enol}) ppm; ^{13}C NMR (50 MHz, DMSO-d_6): δ = 21.5, 60.9, 120.2, 124.6, 128.9, 129.0, 129.2, 130.0, 130.2, 133.1, 135.1, 135.7, 144.3, 149.6, 165.0, 172.5 and 180.6 ppm; ESI-MS: *m/z* (%) = 430 $[M]^+$. Calcd for $C_{21}H_{13}Cl_2NO_3S$ (%): C 58.62, H 3.05, N 3.26; found: C 58.68, H 3.02, N 3.25.

4.2.12. 3-Hydroxy-1-(4-chlorophenyl)-4-(2-thienylcarbonyl)-5-(4-bromophenyl)-2,5-dihydro-1H-pyrrol-2-one (D12)

White powder; yield: 80%; mp = 230 °C; IR (KBr): ν 3161, 1711, 1670, 1606, 1492, 1412, 1371, 1279, 1284, 1092, 988, 831, 759, 722 cm^{-1}; ^1H NMR (200 MHz, DMSO-d_6): δ = 6.34 (s, 1H, CH), 7.18–7.28 (m, 3H, CH_{Ar}), 7.35–7.43 (m, 2H, CH_{Ar}), 7.47–7.54 (m, 2H, CH_{Ar}), 7.56–7.65 (m, 2H, CH_{Ar}), 7.96 (dd, 1H, *J* = 4.9, 1.1 Hz, CH_{Ar}), 8.09 (dd, 1H, *J* = 3.8, 1.1 Hz, CH_{Ar}), 11.96 (br. s, 1H, OH_{enol}) ppm; ^{13}C NMR (50 MHz, DMSO-d_6): δ = 21.5, 60.9, 118.3, 120.3, 124.9, 128.9, 129.0, 130.1, 132.1, 133.1, 135.1, 135.6, 135.7, 135.9, 144.3, 149.6, 165.0, 172.5 and 180.6 ppm; ESI-MS: *m/z* (%) = 475 $[M]^+$. Calcd for $C_{21}H_{13}BrClNO_3S$ (%): C 53.13, H 2.76, N 2.95; found: C 53.22, H 2.74, N 2.96.

4.2.13. 3-Hydroxy-1-(3-nitrophenyl)-4-(2-thienylcarbonyl)-5-(4-(benzyloxy)phenyl)-2,5-dihydro-1H-pyrrol-2-one (D13)

Yellow powder; yield: 73%; mp = 209 °C; IR (KBr): ν 3159, 1681, 1666, 1606, 1496, 1414, 1383, 1243, 1172, 1091, 984, 846, 755, 715 cm^{-1}; ^1H NMR (200 MHz, DMSO-d_6): δ = 4.92 (s, 2H, OCH_2), 6.28 (d, 1H, *J* = 4.5 Hz, CH), 6.82 (d, 2H, *J* = 8.5 Hz, CH_{Ar}), 7.16–7.52 (m, 10H, CH_{Ar}), 7.61–7.73 (m, 2H, CH_{Ar}), 7.97–8.07 (m, 2H, CH_{Ar}), 11.68 (br. s, 1H, OH_{enol}) ppm; ^{13}C NMR (50 MHz, DMSO-d_6): δ = 61.2, 115.0, 124.7, 128.2, 128.3, 128.6, 128.8, 129.0, 129.1, 129.5, 129.6, 129.9, 132.3, 135.1, 135.6, 135.7, 137.3, 144.4, 149.0, 158.6, 165.0 and 180.9 ppm; ESI-MS: *m/z* (%) = 513 $[M]^+$. Calcd for $C_{28}H_{20}N_2O_6S$ (%): C 65.62, H 3.93, N 5.47; found: C 65.71, H 3.91, N 5.44.

4.2.14. 3-Hydroxy-1-(4-nitrophenyl)-4-(2-thienylcarbonyl)-5-(4-(benzyloxy)phenyl)-2,5-dihydro-1H-pyrrol-2-one (D14)

Yellow powder; yield: 77%; mp = 242 °C; IR (KBr): ν 3226, 1689, 1678, 1609, 1512, 1338, 1248, 1172, 988, 859, 753, 722 cm^{-1}; ^1H NMR (200 MHz, DMSO-d_6): δ = 4.91 (s, 2H, OCH_2), 6.38 (s, 1H, CH), 6.83 (d, 2H, *J* = 8.6 Hz, CH_{Ar}), 7.20–7.35 (m, 8H, CH_{Ar}), 7.89–8.08 (m, 4H, CH_{Ar}), 8.18 (d, 2H, *J* = 9.2 Hz, CH_{Ar}) ppm; ^{13}C NMR (50 MHz, DMSO-d_6): δ = 60.8, 69.4, 114.8, 121.2, 122.0, 124.4, 127.5, 127.9, 128.5, 128.7, 129.1, 134.9, 135.5, 136.9, 142.2, 143.6, 143.8, 147.9, 158.2, 165.3 and 180.4 ppm; ESI-MS: *m/z* (%) = 513 $[M]^+$. Calcd for $C_{28}H_{20}N_2O_6S$ (%): C 65.62, H 3.93, N 5.47; found: C 65.70, H 3.92, N 5.49.

4.2.15. 3-Hydroxy-1-(4-chlorophenyl)-4-(2-thienylcarbonyl)-5-(4-(benzyloxy)phenyl)-2,5-dihydro-1H-pyrrol-2-one (D15)

Yellow powder; yield: 79%; mp = 205 °C; IR (KBr): ν 3178, 1682, 1667, 1607, 1512, 1496, 1384, 1244, 1173, 1092, 985, 847, 756, 716 cm^{-1}; ^1H NMR (200 MHz, DMSO-d_6): δ = 4.93 (s, 2H, OCH_2), 6.28 (s, 1H, CH), 6.83 (d, 2H, *J* = 8.8 Hz, CH_{Ar}), 7.21–7.39 (m, 10H, CH_{Ar}), 7.67 (d, 2H, *J* = 8.9 Hz, CH_{Ar}), 7.97 (d, 1H, *J* = 4.9 Hz, CH_{Ar}), 8.07 (d, 1H, *J* = 3.8 Hz, CH_{Ar}), 11.93 (s, 1H, OH_{enol}) ppm; ^{13}C NMR (50 MHz, DMSO-d_6): δ = 61.2, 69.7, 115.0, 115.8, 120.8, 124.7, 128.1, 128.2, 128.3, 128.6, 128.8, 129.0, 129.1, 129.5, 129.8, 132.3, 135.1, 135.6, 135.7, 137.3, 144.4, 149.0, 158.6, 165.0 and 180.8 ppm; ESI-MS: *m/z* (%) = 502 $[M]^+$. Calcd for $C_{28}H_{20}ClNO_4S$ (%): C 66.99, H 4.02, N 2.79; found: C 67.04, H 3.99, N 2.77.

4.3. X-ray crystal structure determination

Single-crystal X-ray diffraction data for **D2** were collected at an Oxford Gemini S diffractometer equipped with a CCD detector, using monochromatized Mo*K*α radiation (λ = 0.71073 Å). Data reduction and empirical absorption correction were performed with CrysAlisPRO [46]. The structure was solved by direct methods using SHELXS and refined on F^2 by full-matrix least-squares using SHELXL [47]. All non-

hydrogen atoms were refined anisotropically. One of two DMSO molecules is disordered over two positions of the S3 atom with occupation numbers of 0.653 and 0.347.

The H atom bonded to the O2 atom from hydroxyl group was located in difference Fourier map and refined isotropically. The rest of the H atoms were placed in geometrically calculated positions and refined using the riding model with U_{iso} values constrained to $1.2U_{eq}$ or $1.5U_{eq}$ of the parent C atoms. The PARST [48] and PLATON [49] software were used to perform the geometrical calculation, while ORTEP3 [50] and was employed for molecular graphics. Crystallographic details for structure analysis of the **D2** compound are summarized in Table S2.

4.4. Cell lines and culture

Healthy human fetal lung fibroblasts (MRC-5) and two human cancer cell lines: cervix adenocarcinoma cells (HeLa) and breast adenocarcinoma cells (MDA-MB 231) were used for cytotoxicity screening of fifteen, previously synthesized, organic compounds. All cell lines were purchased from American Type Culture Collection (ATTC).

Mantainence of HeLa and MRC-5 were carried out using Dulbecco's modified Eagle's medium (DMEM), while MDA-MB 231 was maintained in Roswell Park Memorial Institute medium (RPMI-1640). Both mediums were supplemented with 10% heath-inactivated fetal bovine serum (FBS), L-glutamine (2 mM), non-essential amino acids (0,1 mM), penicillin (100 IU/ml) and streptomycin (100 μg/ml). Cells were kept as a monolayer culture in 25 cm^2 plastic flasks (Greiner Bio-One, Austria) under standard culture conditions of 37 °C, humidified air and 5% CO_2. The media was changed every three days and cells were subcultured when necessary (0.05% trypsin −0.53 mM EDTA). Depending on the type of experiment, cells were seeded in 96- or 24-well microtirar plates (Thermo Scientific, New York, NY).

4.5. Cytotoxicity assays

Effects of 3-hydroxy-3-pyrrolin-2on derivates (**D1**-**D15**) on HeLa, MDA-MB 231 and MRC-5 cells viability were evaluated by two colorimetric assays: MTT (3-(4,5-dimethylthiazol-2-yl)-2,5-diphenyltetrazolium bromide) and SRB (sulforhodamine B). In all experiments, cells were plated in 96-well plates at the density of $3x10^3$ cells per well and incubated to adhere overnight.

4.6. MTT assay

The MTT assay, based on the reduction of the yellow tetrazolium salt to a purple formazan dye by succinate-tetrazolium reductase, which exists in the mitochondrial respiratory chain and is active only in viable cells, was firstly described by Moshman [30]. After adherence, in the first stage (screening), medium was removed and cells were treated with synthesized compounds (**D1**-**D15**) in single dose at concentration 100 μM or media alone, and in the second stage, with selected compounds which exhibited the best inhibitory effect in screening stage, at concentration 1 μM, 3 μM, 10 μM, 30 μM, 100 μM or media alone. After 24 h and 48 h incubation with tested compounds, the medium was replaced with 100 μL of MTT (0.5 mg/mL PBS) and incubated for at least 2 h. Thereafter, colored formazan crystals were dissolved with 150 μL of DMSO. Absorbance was measured at 590 nm with a multiplate reader (Zenyth 3100, Anthos Labtec Instruments GmbH, Austria). Cytotoxicity was calculated according to the formula: $(1\text{-}A_{test}/A_{control}) \times 100$. The IC_{50} values of compounds were calculated using Microsoft Office Excel free add-in ED50plus v1.0 software downloaded from: http://www.sciencegateway.org/protocols/cellbio/drug/data/.

4.7. SRB assay

Cytotoxicity was assessed by SRB assay as described by Skehan et al. [31] Effects of the selected 3-hydroxy-3-pyrrolin-2-on derivatives on cell viability was examined on HeLa, MDA-MB 231 and MRC-5 in concentration of 1 μM, 3 μM, 10 μM, 30 μM, 100 μM during 24 h and 48 h period of incubation. The method of plating and incubation was identical as it was in MTT until the end of incubation. Briefly, treatment was terminated by through fixing cells with 100 μL 10% triacetic acid (TCA) for 1 h at +4 °C. This was followed by five washings with distilled water and staining using 0.1% SRB dissolved in 1% acetic acid at least for 15 min on room temperature. Subsequently, plates were washed four times with 1% acetic acid, air-dried and bound dye was solubilized with 150 μL 10 mM unbuffered Tris base (pH = 10.4) for 5 min on the gyratory shaker. Absorbance was measured at 510 nm with a multiplate reader (Zenyth 3100, Anthos Labtec Instruments GmbH, Austria). Cytotoxicity and IC_{50} were calculated according to the same formula as for MTT assay.

4.8. Flow cytometric analysis

HeLa and MDA-MB 231 cells were cultured overnight for adherence in 24-well plates at a density 1×10^5 per well. Cells were treated with the selected 3-hydroxy-3-pyrrolin-2-ones in concentrations corresponding to their IC_{50} values or in media alone (control) during 48 h at 37 °C in an atmosphere of 5% CO_2 and absolute humidity. In some experiments, 20 μM chloroquine (CQ) was added to both untreated and treated cells 24 h after addition of tested substances. After incubation, the cell was collected and examined for the type of cell death and cell cycle perturbations induced by selected organic compounds.

4.9. Annexin V-FITC/7-AAD assay

According to the manufacturer's instruction, Annexin V-FITC/7-AAD Kit (Beckman Coulter, USA) was used to determine a type of cell death induced by the selected 3-hydroxy-3-pyrrolin-2-ones. After designated treatment, both attached and detached HeLa and MDA-MB 231 cells were collected and washed in PBS. Afterward, cells were resuspended in 100 μL of ice-cold binding buffer (1×10^5/100 μL), stained with 10 μL of Anexin V-FITC and 20 μL 7AAD and incubated in dark on room temperature for 15 min. Finally, Binding buffer (400 μL) was added to each tube and the samples were analyzed by flow cytometer Cytomics FC500 (Beckman Coulter, USA). Data for different cell populations (viable, necrotic, early and late apoptotic cells) were analyzed using Flowing Software (http://www.flowingsoftware.com/) and presented by dot plots.

4.10. Cell cycle analysis

After treatment, as previously described, perturbation of cell cycle was examined for HeLa and MDA-MB 231 cells. Briefly, cells were collected, washed in PBS and fixed overnight with 1 ml of ice-cold 70% ethanol at +4 °C. Then, cells were washed, resuspended in PBS with the addition of RNase A (500 μg/ml PBS) and incubated for 30 min at 37 °C, followed by staining with 5 μL of propidium iodide (10 mg/ml PBS) during 15 min in dark. After incubation, samples were analyzed by flow cytometer Cytomic F500 and the data were analyzed using FlowJo Software. Results were presented by histograms.

4.11. Detection and quantification of acidic vesicular organelles (AVOs) with acridine orange

Acridine orange is cell permeable fluorescent dye that, excited by blue light, emits green fluorescence when it is localized in cytoplasm and nucleus, but emits red fluorescence within compartments with low pH, lysosomes, and phagolysosomes. For autophagy detection, treated and untreated (control) HeLa and MDA-MB 231 cells were trypsinized, washed in PBS and stained with acridine orange (1 mg/ml) for 15 min. Thereafter cells were washed in PBS and analyzed by flow cytometer Cytomic F500. The data were analyzed using Flowing Software.

Accumulation of acidic vacuoles (AVOs) was quantified as red/green fluorescence ratio, i.e. the proportion of mean red and green fluorescence intensity (FL3/FL1).

4.12. Viscosity measurements

The viscosity of aqueous DNA solution was measured in the presence of increasing amounts of **D13** and **D15** using Ubbelohde viscosimeter (SI Analytics GmbH, Mainz, Germany, type no. 525 03) by measuring the flow rate. Viscosimeter was filled with experimental liquid and placed vertically in a glass-sided thermostat maintained constant to ± 0.01 K, with a standard uncertainty of controlled temperature of ± 0.02 K. Flow time was recorded with a digital stopwatch with a digital stopwatch with an accuracy of ± 0.001 s, after thermal equilibrium was obtained. All measurements were performed at 310.15 K. Results were obtained as the mean value of at least ten viscosity measurements, and the mean value of flow time was considered for further analysis. The viscosity values were calculated from the observed flow time of DNA containing solutions (t) corrected for that of buffer alone (t_o), $\eta = (t\text{-}t_0)/t_0$. The obtained data were presented as $(\eta/\eta_0)^{1/3}$ against R, where η is the viscosity of DNA in the presence of ligand, η_o is the viscosity of DNA alone in the buffer solution, and R is mole ratio of ligands/DNA. The DNA concentration was fixed at $1 \cdot 10^{-5}$ mol dm^{-3}. The relative standard uncertainty of determining the viscosity with Ubbelohde viscosimeter did not exceed 1%.

4.13. Computational method

For the docking procedure, the crystallographic 3-dimensional structures of B-DNA dodecamer and bovine serum albumin (BSA) were obtained from the protein data bank, PDB ID: 1BNA and 3V03, respectively. The receptors were prepared using the protein preparation wizard by involving parameters like assigning bond orders to hydrogens, capping the termini and desolvation by deleting the crystallized free water molecules beyond 5 Å. The validity of the structure was checked and adjusted by adding missing residues and loops applying Prime included in the Schrödinger suite package [51]. The protonation and tautomeric states of residues were adjusted to match pH of 7 using PROPKA [52]. The DNA and BSA hydrogen bonds were optimized and minimized applying the force field OPLS 2005 [53]. The Glide module was used for generation of receptor-active pocket and this was further used for the docking studies [54].

Receptor and ligand docking studies were carried out using the ligand docking module from the glide application in the Schrödinger suite. This module is a grid-based method and gives scores based on the formation of favorable interactions between ligand and receptor. The prepared ligands were docked into the grid enclosed active pocket of the protein using the extra precision mode. Flexible ligand sampling was applied in the docking procedure. The receptor-ligand complex interactions were calculated based on the quality of geometric contacts and their energy. All poses were subjected to post-docking minimization. The best-docked structures for each ligand were determined, based on the model energy score which combines the energy grid score, the binding affinity, the internal strain energy, and the Coulomb-van der Waals interaction energy scores [55].

Acknowledgments

The authors are grateful to the Ministry of Education, Science and Technological Development of the Republic of Serbia for financial support (Grant 172011).

Appendix A. Supplementary material

Supplementary data to this article can be found online at https://doi.org/10.1016/j.bioorg.2019.102954.

References

[1] S.D. Schaefer, J.D. Post, L.G. Close, C.G. Wright, Ototoxicity of low- and moderate-dose cisplatin, Cancer 56 (1985) 1934–1939.
[2] M.P. Goren, R.K. Wright, M.E. Horowitz, Cumulative renal tubular damage associated with cisplatin nephrotoxicity, Cancer Chemother. Pharmacol. 18 (1986) 69–73.
[3] D.S. Alberts, J.K. Noel, Cisplatin-associated neurotoxicity: can it be prevented? Anticancer Drugs 6 (1995) 369–383.
[4] M. Kartalou, J.M. Essigmann, Mechanisms of resistance to cisplatin, Mutat. Res. 478 (2001) 23–43.
[5] M.A. Fuertes, M. Alonso, J.M. Pérez, Biochemical modulation of cisplatin mechanisms of action: enhancement of antitumor activity and circumvention of drug resistance, Chem. Rev. 103 (2003) 645–662.
[6] I. Ott, R. Gust, Non platinum metal complexes as anti-cancer drugs, Arch. Pharm. 340 (2007) 117.
[7] S.S. Zimmerman, A. Khatri, E.C. Garnier-Amblard, P. Mullasseril, N.L. Kurtkaya, S. Gyoneva, K.B. Hansen, S.F. Traynelis, D.C. Liotta, Design, synthesis, and structure – activity relationship of a novel series of GluN2C-selective potentiators, J. Med. Chem. 57 (2014) 2334–2356.
[8] V.L. Gein, V.N. Vychegzhanina, E.B. Levandovskaya, B.Ya. Syropyatov, M.I. Vakhrin, E.V. Voronina, N.V. Danilova, Synthesis and antibacterial and analgesic activity of 5-aryl-4-acyl-3-hydroxy-1(2,2-dimethoxyethyl)-3-pyrrolin-2-ones, Pharm. Chem. J. 44 (2010) 370–373.
[9] V.L. Gein, V.S. Platonov, É.V. Voronina, Synthesis and antimicrobial activity of 1,5-diaryl-4-heteroyl-3-hodroxy-3-pirolin-2-ones, Pharm. Chem. J. 38 (2004) 316–318.
[10] V.L. Gein, V.A. Mihalev, N.N. Kasimova, E.V. Voronina, M.I. Vakhrin, E.B. Babushkina, Synthesis and antibacterial activity of 1-alxoxyalkyl-5-aryl-4-acyl-3-hydroxy-3-pyrrolin-2-ones, Pharm. Chem. J. 41 (2007) 208–210.
[11] L. Gein, A.A. Bobyleva, E.B. Levandovskaya, T.F. Odegova, M.I. Vakhrin, Synthesis and antimicrobial activity of 5-aryl-4-acyl(heteroyl)-3-hydroxy-1-(3-ethoxypropyl)-3-pyrrolin-2-ones, Pharm. Chem. J. 46 (2012) 23–25.
[12] V.L. Gein, T.F. Odegova, S.N. Rogachev, A.A. Bobyleva, L.F. Gein, Synthesis and antimicrobial activity of 5-aryl-4-acyl-3-hydroxy-1-[2-(3-hidrohyethoxy)-ethyl]-3-pyrrolin-2-ones, Pharm. Chem. J. 49 (2015) 175–177.
[13] V.L. Gein, E.V. Shumilovskikh, Yu.S. Andreichikov, R.F. Saraeva, L.V. Korobchenko, G.V. Vladyko, E.I. Boreko, Synthesis of 4-substituted 1-methyl-5-aryl- and 1,5-diaryltetrahydropyrrole-2,3-diones and their antiviral action, Pharm. Chem. J. 25 (1991) 884–887.
[14] V.L. Gein, O.V. Voronina, T.E. Ryumina, G.N. Novoselova, K.D. Potemkin, Y.S. Andreichikov, Synthesis and antimicrobial activity of 1,5-diaryl-3-hydroxy-2-oxo-3-pyrroline-4-carboxylic acids and their derivatives, Pharm. Chem. J. 30 (1996) 95–96.
[15] V.L. Gein, A.V. Popov, V.É. Kolla, N.A. Popova, K.D. Potemkin, Synthesis and biological activity of 1,5-diaryl-3-arylamino-4-carboxymethyl-2,5-dihydro-2-pyrrolones and 1,5-diaryl-4-carboxymethyltetrahydropyrrole-2, 3-diones, Pharm. Chem. J. 27 (1993) 343–346.
[16] A. Divsalar, A.A. Saboury, H. Mansouri-Torshizi, A.A. Moosavi-Movahedi, Binding properties of a new anti-tumor component (2,2′-bipyridin octylglycinato Pd(II) nitrate) with Bovine β-lactoglobulin-A and –B, J. Biomol. Struct. Dyn. 25 (2007) 173–182.
[17] L.T. Bozic, M. Juribasic, P. Traldi, V. Scarcia, A. Furlani, Synthesis, characterization and antitumor activity of palladium(II) complexes of monoethyl 8-quinolylmethylphosphonate, Polyhedron 27 (2008) 1317–1328.
[18] H. Mansouri-Torshizi, M. Saeidifar, A. Divsalar, A.A. Saboury, S. Shahraki, Interaction studies of a novel, water-soluble and anti-cancer palladim(II) complex with calf thymus DNA, Bull. Korean Chem. Soc. 31 (2010) 435–441.
[19] C.J. Burrows, S.E. Rokita, Recognition of guanine structure in nucleic acids by nickel complexes, Acc. Chem. Res. 27 (1994) 295–301.
[20] N. Poklar, D.S. Pilch, S.J. Lippard, E.A. Redding, S.U. Dunham, K.J. Breslauer, Influence of cisplatin intrastrand crosslinking on the conformation, thermal stability, and energetics of a 20-mer DNA duplex, Proc. Natl. Acad. Sci. U. S. A. 93 (1996) 7606–7611.
[21] G.B. Onoa, V. Moreno, Palladium and platinum famotidine complexes, J. Inorg. Biochem. 72 (1998) 141–153.
[22] R. Kieltyka, J. Fakhoury, N. Moitessier, H.F. Sleiman, Platinum phenanthroimidazole complexes as G-quadruplex DNA selective binders, Chem. - Eur. J. 14 (2008) 1145–1154.
[23] N.H. Campbell, N.H.A. Karim, G.N. Parkinson, M. Gunaratnam, V. Petrucci, A.K. Todd, R. Vilar, S. Neidle, Molecular basis of structure-activity relationships between salphen metal complexes and human telomeric DNA quadruplexes, J. Med. Chem. 55 (2012) 209–222.
[24] N.H. Abd Karim, O. Mendoza, A. Shivalingam, A.J. Thompson, S. Ghosh, M.K. Kuimova, R. Vilar, Salphen metal complexes as tunable G-quadruplex binders and optical probes, RSC Adv. 4 (2014) 3355–3363.
[25] K. Takahashi, K. Fukiura, H. Arii, M. Chikira, Design of salen-type Ni(II) complexes for recognition of DNA base sequence, Nucleic Acids Symp. Ser. (Oxf) 51 (2007) 189–190.
[26] M.A. Bork, C.G. Gianopoulos, H. Zhang, P.E. Fanwick, J.H. Choi, D.R. McMillin, Accessibility and external versus intercalative binding to DNA as assessed by oxygen-induced quenching of the palladium(II)-containing cationic porphyrins Pd(T4) and Pd(tD4), Biochem. 53 (2014) 714–724.
[27] A. Lauria, R. Bonsignore, A. Terenzi, A. Spinello, F. Giannici, A. Longo, A.M. Almerico, G. Barone, Nickel(II), copper(II) and zinc(II) metallo-intercalators: structural details of the DNA-binding by a combined experimental and

computational investigation, Dalton Trans. 43 (2014) 6108–6119.
[28] K.D. Demertzi, M.A. Demertzis, E. Filiou, A.A. Pantazaki, P.N. Yadav, J.R. Miller, Y. Zheng, D.A. Kyriakidis, Platinum(II) and palladium(II) complexes with 2-Acetyl pyridine 4N-ethyl thiosemicarbazone able to overcome the *cis*-Platin resistance.Structure, antibacterial activity and DNA strand breakage, Biometals 16 (2003) 411–418.
[29] V.L. Gein, M.A. Mar'yasov, Reactions of 5-Aryl-4-(hetaren-2-ylcarbonyl)-3-hydroxy-1-(1,3-thiazol-2-yl)-2,5-dihydro-1H-pyrrol-2-ones with Hydrazine, Phenylhydrazine, and Hydroxylamine, Russ. J. Org. Chem. 51 (2015) 110–115.
[30] T. Mosmann, Rapid colorimetric assay for cellular growth and survival: Application to proliferation and cytotoxicity assays, J. Immunol. Methods. 65 (1983) 55–63.
[31] P. Skehan, R. Storeng, D. Scudiero, A. Monks, J. McMahon, D. Vistica, J.T. Warren, H. Bokesch, S. Kenney, M.R. Boyd, New colorimetric cytotoxicity assay for anticancer-drug screening, J. Natl. Cancer. Inst. 82 (1990) 1107–1112.
[32] S.-Z. Rena, Z.-C. Wanga, X.-H. Zhua, D. Zhua, Z. Lia, F.-Q. Shena, Y.-T. Duanc, H. Caoa, J. Zhaob, H.-L. Zhua, Design and biological evaluation of novel hybrids of 1,5-diarylpyrazole and Chrysin for selective COX-2 inhibition, Bioorg. Med. Chem. 26 (2018) 4264–4275.
[33] L. Leite, D. Jansone, I. Shestakova, I. Domracheva, N. Veretennikova, E. Lukevics, G. Melikyan, Synthesis and antitumor effect of aryl(heteryl) gamma- and sigma-lactones, Drugs Future 27 (Suppl A) (2002) P336 (abstr).
[34] A. Nersesyan, G.S. Melikyan, H. Stopper, The study of genotoxicity of two newly synthesized pyrrolinone derivatives on L5178Y mouse lymphoma nad bone marrow cells, Exp. Oncol. 25 (2003) 176–179.
[35] P. Mowery, F. Banales Mejia, C.L. Franceschi, M.H. Kean, D.O. Kwansare, M.M. Lafferty, N.D. Neerukonda, C.E. Rolph, N.J. Truax, E.T. Pelkey, Synthesis and evaluation of the anti-priliferative activity of diaryl-3-pyrrolin-2-ones and fused analogs, Bioorg. Med. Chem. Lett. 27 (2016) 191–195.
[36] R.S.Y. Wong, Apoptosis in cancer: from pathogenesis to treatment, J. Exp. Clin. Cancer Res. 30 (1) (2011) 87, https://doi.org/10.1186/1756-9966-30-87.
[37] E. White, Deconvoluting the context-dependent role for autophagy in cancer, Nat. Rev. Cancer 12 (2012) 401–410.
[38] J. Olmsted, R.D. Kearns III, Mechanism of ethidium bromide fluorescence enhancement on binding to nucleic acids, Biochem. 16 (1977) 3647–3654.
[39] N. Janković, J. Muškinja, Z. Ratković, Z. Bugarčić, B. Ranković, M. Kosanić, S. Stefanović, Solvent-free synthesis of novel vaillidene derivatives of Meldrum's acid: biological evaluation, DNA and BSA binding study, RSC Adv. 6 (2016) 39452–39459.
[40] R. Lakowicz, G. Weber, Quenching of fluorescence by oxygen. Probe for structural fluctuations in macromolecules, Biochem. 12 (1973) 4161–4170.
[41] J. Petronijević, N. Janković, T.P. Stanojković, N. Joksimović, N.Đ. Grozdanić, M. Vraneš, A. Tot, Z. Bugarčić, Biological evaluation of selected 3,4-dihydro-2(1H)-quinoxalinones and 3,4-dihydro-1,4-benzoxazin-2-ones: molecular docking study, Arch. Pharm. Chem. Life Sci. (2018) 1–13, https://doi.org/10.1002/ardp.201700308.
[42] L. Strekowski, B. Wilson, Noncovalent interactions with DNA: an overview, Mut. Res. 623 (2007) 3–13.
[43] T. Topală, A. Bodoki, L. Oprean, R. Oprean, Bovine Serum Albumin Interactions with Metal Complexes, Clujul. Med. 87 (2014) 215–219.
[44] J.R. Brown, Albumin Structure, Function and Uses in: V.M. Rosenoer, M. Oratz, M. A. Rothschild (Eds.), Pergamon, Oxford, 1977, pp. 27–51.
[45] N. Joksimović, D. Baskić, S. Popović, M. Zarić, M. Kosanić, B. Ranković, T. Stanojković, B.S. Novaković, G. Davidović, Z. Bugarčić, N. Janković, Synthesis, characterization, biological activity, DNA and BSA binding study: novel copper(II) complexes with 2-hydroxy-4-aryl-4- oxo-2-butenoate, Dalton Trans. 45 (2016) 15067–15077.
[46] CrysAlisPRO Software system, Agilent Technologies UK Ltd., Oxford, England, 2014.
[47] G.M. Sheldrick, Crystal structure refinement with SHELXL, Acta Crystallogr. C 71 (2015) 3–8.
[48] M. Nardelli, PARST95 – an update to PARST: a system of Fortran routines for calculating molecular structure parameters from the results of crystal structure analyses, J. Appl. Crystallogr. 28 (1995) 659.
[49] A.L. Spek, Single-crystal structure validation with the program PLATON, J. Appl. Crystallogr. 36 (2003) 7–13.
[50] L.L.J. Farrugia, WinGX and ORTEP for Windows: an update, J. Appl. Crystallogr. 45 (2012) 849–854.
[51] Schrödinger Suite 2015, Protein Preparation Wizard. Schrödinger, LLC; New York, NY.
[52] M. Rostkowski, M. Olsson, C. Sondergaard, J. Jensen, Graphical analysis of pH-dependent properties of proteins predicted using PROPKA, BMC Struct. Bio. 11 (2011) 1–6.
[53] W.L. Jorgensen, J. Tirado-Rives, Potential energy functions for atomic-level simulations of water and organic and biomolecular systems, Proc. Natl. Acad. Sci. USA 102 (2005) 6665–6670.
[54] Schrödinger Suite 2015, Glide, Schrödinger, LLC; New York, NY.
[55] K.M. Elokely, R.J. Doerksen, Docking challenge: protein sampling and molecular docking performance, J. Chem Inf. Model. 53 (2013) 1934–1945.